



Combined Search for the Standard Model Higgs Boson from the DØ Experiment in up to 9.7 fb^{-1} of Data

The DØ Higgs Group

(Dated: March 6, 2012)

Searches for standard model Higgs boson production in $p\bar{p}$ collisions at $\sqrt{s} = 1.96 \text{ TeV}$ are carried out for Higgs boson masses (m_H) in the range $100 \leq m_H \leq 200 \text{ GeV}/c^2$. The contributing production processes include gluon-gluon fusion ($gg \rightarrow H$), associated production ($q\bar{q} \rightarrow VH$) and vector boson fusion ($q\bar{q} \rightarrow q\bar{q}H$). Analyses are conducted over an array of distinct final states with integrated luminosities ranging from 4.3 to 9.7 fb^{-1} . We set limits on standard model Higgs boson production. The observed 95% Confidence Level upper limits are found to be a factor of 2.17 (0.94) times the predicted standard model cross section at $m_H = 115$ (165) GeV/c^2 , while the expected limit is found to be a factor of 1.58 (0.76) times the standard model prediction for the same mass. We exclude at the 95% C.L. the region $159 < m_H < 166 \text{ GeV}/c^2$ with an *a priori* expected exclusion of $157 < m_H < 172 \text{ GeV}/c^2$. In the mass range $\sim 115 - 145 \text{ GeV}/c^2$, the data exhibit an excess above the background prediction at the level of 1–2 Gaussian standard deviations.

Preliminary Results for Winter 2012 Conferences

I. INTRODUCTION

Despite its success as a predictive tool, the standard model (SM) of particle physics remains incomplete without a means to explain electroweak symmetry breaking. The simplest proposed mechanism involves the introduction of a complex doublet of scalar fields that generate the masses of elementary particles via their mutual interactions. After accounting for longitudinal polarizations for the electroweak bosons, this so-called Higgs mechanism also gives rise to a single scalar boson with an unpredicted mass. Direct searches in $e^+e^- \rightarrow Z^* \rightarrow ZH$ at the Large Electron Positron (LEP) collider yielded a lower mass limit at $m_H > 114.4 \text{ GeV}/c^2$ [1] while precision electroweak data yield the indirect constraint $m_H < 161 \text{ GeV}/c^2$ [2], with both limits set at 95% confidence level (C.L.). When also considering the limit from LEP, the precision electroweak measurements predict $m_H < 185 \text{ GeV}/c^2$, indicating that the range $100 \leq m_H \leq 200 \text{ GeV}/c^2$ is the most important search region for a SM Higgs boson. Recent results from the CMS [3] and ATLAS [4] experiments now limit the SM Higgs boson to have a mass between 115.5 GeV and 127 GeV at 95% C.L.

In this note, we combine the results of direct searches for SM Higgs bosons in $p\bar{p}$ collisions at $\sqrt{s} = 1.96 \text{ TeV}$ recorded by the DØ experiment [5]. The analyses combined here seek signals of Higgs bosons produced through gluon-gluon fusion (GGF) ($gg \rightarrow H$), in association with vector bosons ($q\bar{q} \rightarrow VH$, where $V = W, Z$), and through vector boson fusion (VBF) ($q\bar{q} \rightarrow q\bar{q}H$). The analyses utilize data corresponding to integrated luminosities ranging from 4.3 to 9.7 fb^{-1} , collected during the data taking period 2002-2011 (Run II). The Higgs boson decay modes studied are $H \rightarrow b\bar{b}$, $H \rightarrow W^+W^-$, $H \rightarrow ZZ$, $H \rightarrow \tau^+\tau^-$, and $H \rightarrow \gamma\gamma$. The searches are organized into analysis sub-channels comprising different production, decay, and final state particle configurations, each designed to maximize the sensitivity for a particular Higgs boson production and decay mode. In order to facilitate proper combination of signals, the analyses were constructed to be mutually exclusive after analysis selections.

The analyses used in this combination [6–15] are outlined in Table I. In the cases of $p\bar{p} \rightarrow VH$ production, we search for a Higgs boson decaying to two bottom quarks, two tau leptons, two photons, or two W bosons. The decays of the vector bosons further define the analyzed final states. To isolate $H \rightarrow b\bar{b}$ decays, an algorithm for identifying jets consistent with containing the decay of a b -quark is applied to each jet (b -tagging). Several kinematic variables sensitive to displaced jet vertices and jet tracks with large transverse impact parameters relative to the hard-scatter vertices are combined in a new boosted decision tree based b -tagging discriminant. The new algorithm is an upgraded version of the neural network b -tagger used previously [17]. By adjusting a minimum requirement on the b -tagging output, a spectrum of increasingly stringent b -tagging operating points is achieved, each with a different signal efficiency and purity. The $ZH \rightarrow \ell b\bar{b}$ ($\ell = e, \mu$) analysis requires that at least one jet passes a tight b -tag requirement. The events are further divided into “double-tag” and “single-tag” sub-channels depending on whether or not there is another jet that passes a loose b -tag requirement. A typical per-jet efficiency and fake rate for the loose (tight) b -tag selection is about 80% (50%) and 10% (1%), respectively. The $WH \rightarrow \ell \nu b\bar{b}$ analyses define a single-tag sub-channel similar to $ZH \rightarrow \ell b\bar{b}$, however, events with two b -tags are further divided into either a loose double-tag or tight double-tag category, for a total of three b -tag sub-channels (per lepton flavor and jet multiplicity). The $ZH \rightarrow \nu \bar{\nu} b\bar{b}$ analysis uses the sum of the b -tag outputs from the two highest p_T jets to define two orthogonal b -tag sub-channels. The “tight-tag” sub-channel requires that both jets pass rather tight b -tag criteria, while the “medium-tag” sub-channel allows for the criteria on one of the jets to be relaxed provided that the other jet has a sufficiently high b -tag output. Furthermore, the $WH \rightarrow \ell \nu b\bar{b}$ and $ZH \rightarrow \nu \bar{\nu} b\bar{b}$ analyses use the output from the b -tagger as input to final discriminants. The $ZH \rightarrow \nu \bar{\nu} b\bar{b}$ analysis includes the signal contribution from $WH \rightarrow \ell \nu b\bar{b}$ production where the primary lepton from the W boson decay falls outside of the detector fiducial volume or is not identified as a lepton.

We also consider Higgs decays to two W bosons for the three dominant production mechanisms: gluon-gluon fusion, associated production and vector-boson fusion. In all $H \rightarrow W^+W^-$ decays with $m_H < 2m_W$, at least one of the W bosons will be off mass shell. In the case of production via gluon-gluon fusion and vector-boson fusion, we search for leptonic W boson decays with five final states of opposite-signed leptons: $W^+W^- \rightarrow e^+\nu e^-\nu$, $e^\pm\nu\mu^\mp\nu$, $\mu^+\nu\mu^-\nu$, $e^\pm\nu\tau_{had}^\mp\nu$ and $\mu^\pm\nu\tau_{had}^\mp\nu$, where τ_{had} denotes a hadronic tau decay. Leptonic decays of tau leptons are included. In addition we consider final states originating from Higgs boson production in association with a vector boson (WH or ZH), where leptons may originate from the vector boson or Higgs boson decay. We classify events according to their jet multiplicity in order to isolate particular signal production mechanisms and optimize the discrimination between signal and background. The $H \rightarrow W^+W^- \rightarrow \ell^\pm\nu\ell^\mp\nu$ ($\ell = e, \mu$) analyses separate events in three final states with 0 jets, 1 jet, and 2 or more jets. Analyses identifying hadronic tau candidates select events with ≤ 1 jets, mainly sensitive to the gluon-gluon fusion signal, or with ≥ 2 jets, also sensitive to vector-boson fusion. At high Higgs boson masses (above $m_H = 130$), the dominant signal contribution to both tau analyses originates from $H \rightarrow W^+W^- \rightarrow \mu^\pm\nu\tau^\mp\nu$. The tau analyses requiring at least two jets select significant signal at low Higgs masses (below $m_H = 130$) from $ZH \rightarrow \tau\tau b\bar{b}$ and $VH \rightarrow q\bar{q}\tau\tau$. Another analysis considers the semileptonic decay $H \rightarrow W^+W^- \rightarrow \ell\nu q\bar{q}$. For $VH \rightarrow VWW$ production,

we consider final states with three charged leptons ($ee\mu$, $\mu\mu e$, and $\tau\tau\mu$), as well as the dilepton final state containing an electron and muon with the same charge ($e^\pm\mu^\pm + X$), which benefits greatly from the suppression of Drell-Yan background. Finally, we include an analysis that searches for Higgs bosons decaying to two photons and produced via gluon-gluon fusion, vector boson fusion, and associated production mechanisms.

Since the last DØ SM combined Higgs boson search over the this full mass range [18], we have updated the $WH \rightarrow \ell\nu b\bar{b}$, $ZH \rightarrow \nu\bar{\nu} b\bar{b}$, $ZH \rightarrow \ell\bar{\ell} b\bar{b}$, $H \rightarrow W^+W^- \rightarrow \ell^\pm\nu\ell^\mp\nu$, $VH \rightarrow e^\pm\mu^\pm + X$, $H+X \rightarrow \ell^\pm\tau_{had}^\mp jj$, and $H \rightarrow \gamma\gamma$ analyses.

TABLE I: List of analysis channels ($V = W, Z$ and $\ell = e, \mu$) with the corresponding integrated luminosities, final variables used for setting limits, and mass range studied. See Sect. I for details. All conference notes can be found from Ref. [16].

Channel	Luminosity (fb^{-1})	Final Variable	m_H Range	Reference
$WH \rightarrow \ell\nu b\bar{b}$, (3 b -tag categories/2,3 jets)	9.7	Decision Tree Discriminant	100–150	[6]
$ZH \rightarrow \nu\bar{\nu} b\bar{b}$, (2 b -tag categories/2,3 jets)	9.5	Decision Tree Discriminant	100–150	[7]
$ZH \rightarrow \ell\bar{\ell} b\bar{b}$, (2 b -tag categories/2,3 jets)	9.7	Decision Tree Discriminant	100–150	[8]
$H \rightarrow W^+W^- \rightarrow \ell^\pm\nu\ell^\mp\nu$, (0,1,2 jets)	8.6–9.7	Decision Tree Discriminant	115–200	[9]
$VH \rightarrow e^\pm\mu^\pm + X$	9.7	Decision Tree Discriminant	115–200	[12]
$VH \rightarrow ee\mu/\mu\mu e + X$	9.7	Decision Tree Discriminant	100–200	[13]
$VH \rightarrow \tau\tau\mu + X$	7.0	Summed $ p_T $ of all objects	115–200	[14]
$H \rightarrow W^+W^- \rightarrow \ell\nu q\bar{q}$	5.4	Decision Tree Discriminant	155–200	[10]
$H+X \rightarrow \mu^\pm\tau_{had}^\mp + \leq 1j$	7.3	Neural Network Discriminant	115–200	[11]
$H+X \rightarrow \ell^\pm\tau_{had}^\mp jj$	4.3–6.2	Decision Tree Discriminant	105–200	[11]
$H \rightarrow \gamma\gamma$	9.7	Decision Tree Discriminant	100–150	[15]

The backgrounds from multijet production are measured in data. The other backgrounds were generated by PYTHIA [19], ALPGEN [20], and SINGLETOP [21], with PYTHIA providing parton-showering and hadronization. Drell-Yan, W , and diboson background cross sections are normalized either to next-to-leading order (NLO) calculations from MCFM [22] or, when possible, to data control samples. Top pair and single top production are normalized to approximate next-to-next-to-NLO [23] and next-to-next-to-NLO [24] calculations, respectively.

II. SIGNAL PREDICTIONS AND UNCERTAINTIES

A common approach to the signal predictions and associated uncertainties is followed by the CDF and DØ Collaborations. An outline of the procedures followed is given here; more complete discussion can be found in Ref. [25].

The Monte Carlo signal simulation is provided by the LO generator PYTHIA (with CTEQ5L and CTEQ6L1 [26] leading-order (LO) parton distribution functions) which includes a parton shower and fragmentation and hadronization models. We reweight the Higgs boson p_T spectra in the PYTHIA Monte Carlo samples to that predicted by HQT [27] when making predictions of differential distributions of GGF signal events. To evaluate the impact of the scale uncertainty on the differential spectra, we use the RESBOS [28] generator, and apply the scale-dependent differences in the Higgs boson p_T spectrum to the HQT prediction, and propagate these to our final discriminants as a systematic uncertainty on the shape of the final variable distribution, which is included in the calculation of the limits.

We normalize the Higgs boson signal predictions to the most recent higher-order calculations available. The $gg \rightarrow H$ production cross section is calculated at next-to-next-to leading order (NNLO) in QCD with a next-to-next-to leading log (NNLL) resummation of soft gluons; the calculation also includes two-loop electroweak effects and handling of the running b quark mass [29, 30]. The numerical values in Table II are updates [31] of these predictions with m_t set to 173.1 GeV/ c^2 [32], and an exact treatment of the massive top and bottom loop corrections up to NLO + next-to-leading-log accuracy. The factorization and renormalization scale choice for this calculation is $\mu_F = \mu_R = m_H$. These calculations are refinements of the earlier NNLO calculations of the $gg \rightarrow H$ production cross section [33–35]. Electroweak corrections were computed in Refs. [36, 37]. Soft gluon resummation was introduced in the prediction of the $gg \rightarrow H$ production cross section [38]. The $gg \rightarrow H$ production cross section depends strongly on the gluon parton density function, and the accompanying value of $\alpha_s(q^2)$. The cross sections used here are calculated with the MSTW 2008 NNLO PDF set [39], as recommended by the PDF4LHC working group [40]. The inclusive (over jet multiplicity) Higgs boson production cross sections are listed in Table II.

For analyses that consider inclusive $gg \rightarrow H$ production, but do not split the signal prediction into separate channels based on the number of reconstructed jets, we use the inclusive uncertainties from the simultaneous variation of the

factorization and renormalization scale up and down by a factor of two. We use the prescription of the PDF4LHC working group for evaluating PDF uncertainties on the inclusive production cross section. QCD scale uncertainties that affect the cross section via their impact on the PDFs are included as a correlated part of the total scale uncertainty. The remainder of the PDF uncertainty is treated as uncorrelated with the QCD scale uncertainty.

For analyses seeking $gg \rightarrow H$ production that divide events into categories based on the number of reconstructed jets, we employ an approach for evaluating the impact of the scale uncertainties following Ref. [41]. We treat the QCD scale uncertainties obtained from the NNLL inclusive [29, 30], NLO with one or more jets [43], and NLO with two or more jets [44] cross section calculations as uncorrelated with one another. We then obtain QCD scale uncertainties for the exclusive $gg \rightarrow H + 0$ jet, 1 jet, and 2 or more jet categories by propagating the uncertainties on the inclusive cross section predictions through the subtractions needed to predict the exclusive rates. For example, the $H+0$ jet cross section is obtained by subtracting the NLO $H + 1$ or more jet cross section from the inclusive NNLL+NNLO cross section. Therefore, we assign three separate, uncorrelated scale uncertainties which lead to correlated and anticorrelated uncertainty contributions between exclusive jet categories. The procedure in Ref. [43] is used to determine PDF model uncertainties. These are obtained separately for each jet bin and treated as 100% correlated between jet bins.

Another source of uncertainty in the prediction of $\sigma(gg \rightarrow H)$ is the extrapolation of the QCD corrections computed for the heavy top quark loops to the light-quark loops included as part of the electroweak corrections. Uncertainties at the level of 1-2% are already included in the cross section values we use [29, 30]. It has been argued [29] that the factorization of QCD corrections is known to work well for Higgs boson masses much larger than the masses of the particles contributing to the loop. A 4% change in the predicted cross section is seen when all QCD corrections are removed from the diagrams containing light-flavored quark loops, which is too conservative. For the b quark loop [29], the QCD corrections are much smaller than for the top loop, further giving confidence that it does not introduce large uncertainties.

We include all significant Higgs production modes in our searches. Besides GGF through virtual quark loops, we include Higgs boson production in association with a W or Z vector boson, and vector boson fusion. We use the WH and ZH production cross sections computed at NNLO [45]. This calculation starts with the NLO calculation of v2HV [46] and includes NNLO QCD contributions [47], as well as one-loop electroweak corrections [48]. We use the VBF cross section computed at NNLO in QCD [49]. Electroweak corrections to the VBF production cross section are computed with the HAWK program [50], and are very small (0.03 fb and less) for the Higgs boson mass range considered here.

The Higgs boson decay branching ratio predictions are calculated with HDECAY [51], and are also listed in Table II. We use HDECAY Version 3.53. While the HWW coupling is well predicted, $B(H \rightarrow W^+W^-)$ depends on the partial widths of all other Higgs boson decays. The partial width $\Gamma(H \rightarrow b\bar{b})$ is sensitive to m_b and α_s , $\Gamma(H \rightarrow c\bar{c})$ is sensitive to m_c and α_s , and $\Gamma(H \rightarrow gg)$ is sensitive to α_s . The impacts of these uncertainties on $B(H \rightarrow W^+W^-)$ depend on m_H due to the fact that $B(H \rightarrow b\bar{b})$, $B(H \rightarrow c\bar{c})$, $B(H \rightarrow gg)$ become very small for Higgs boson masses above 160 GeV/ c^2 , while they have a larger impact for lower m_H . We use the uncertainties on the branching fraction $B(H \rightarrow W^+W^-)$ from Ref. [52]. At $m_H = 130$ GeV/ c^2 , for example, the m_b variation gives a ${}_{+1.70}^{-4.89}\%$ relative variation in $B(H \rightarrow W^+W^-)$, α_s gives a ${}_{+1.09}^{-1.02}\%$ variation, and m_c gives a ${}_{+0.51}^{-0.45}\%$ variation. At $m_H = 165$ GeV/ c^2 , all three of these uncertainties drop below 0.1%.

III. LIMIT CALCULATIONS

We combine results using the CL_s method with a negative log-likelihood ratio (LLR) test statistic [53]. The value of CL_s is defined as $CL_s = CL_{s+b}/CL_b$ where CL_{s+b} and CL_b are the confidence levels for the signal-plus-background hypothesis and the background-only hypothesis, respectively. These confidence levels are evaluated by integrating corresponding LLR distributions populated by simulating outcomes via Poisson statistics. Separate channels and bins are combined by summing LLR values over all bins and channels. This method provides a robust means of combining individual channels while maintaining individual channel sensitivities and incorporating systematic uncertainties. Systematics are treated as Gaussian uncertainties on the expected number of signal and background events, not the outcomes of the limit calculations. This approach ensures that the uncertainties and their correlations are propagated to the outcome with their proper weights. The CL_s approach used in this combination utilizes binned final-variable distributions rather than a single-bin (fully integrated) value for each contributing analysis. The exclusion criteria are determined by increasing the signal cross section until $CL_s = 1 - \alpha$, which defines a signal cross section excluded at 95% confidence level for $\alpha = 0.95$.

TABLE II: The production cross sections (in fb) and decay branching fractions (in %) for each SM Higgs boson mass (in GeV/ c^2) assumed for the combination.

m_H	$\sigma_{q\bar{q}\rightarrow H}$	σ_{WH}	σ_{ZH}	σ_{VBF}	$B(H \rightarrow b\bar{b})$	$B(H \rightarrow c\bar{c})$	$B(H \rightarrow \tau^+\tau^-)$	$B(H \rightarrow W^+W^-)$	$B(H \rightarrow ZZ)$	$B(H \rightarrow \gamma\gamma)$
100	1821.8	281.10	162.7	100.1	79.1	3.68	8.36	1.11	0.113	0.159
105	1584.7	238.70	139.5	92.3	77.3	3.59	8.25	2.43	0.215	0.178
110	1385.0	203.70	120.2	85.1	74.5	3.46	8.03	4.82	0.439	0.197
115	1215.9	174.50	103.9	78.6	70.5	3.27	7.65	8.67	0.873	0.213
120	1072.3	150.10	90.2	72.7	64.9	3.01	7.11	14.3	1.60	0.225
125	949.3	129.50	78.5	67.1	57.8	2.68	6.37	21.6	2.67	0.230
130	842.9	112.00	68.5	62.1	49.4	2.29	5.49	30.5	4.02	0.226
135	750.8	97.20	60.0	57.5	40.4	1.87	4.52	40.3	5.51	0.214
140	670.6	84.60	52.7	53.2	31.4	1.46	3.54	50.4	6.92	0.194
145	600.6	73.70	46.3	49.4	23.1	1.07	2.62	60.3	7.96	0.168
150	539.1	64.40	40.8	45.8	15.7	0.725	1.79	69.9	8.28	0.137
155	484.0	56.20	35.9	42.4	9.18	0.425	1.06	79.6	7.36	0.100
160	432.3	48.50	31.4	39.4	3.44	0.159	0.397	90.9	4.16	0.0533
165	383.7	43.60	28.4	36.6	1.19	0.0549	0.138	96.0	2.22	0.0230
170	344.0	38.50	25.3	34.0	0.787	0.0364	0.0920	96.5	2.36	0.0158
175	309.7	34.00	22.5	31.6	0.612	0.0283	0.0719	95.8	3.23	0.0123
180	279.2	30.10	20.0	29.4	0.497	0.0230	0.0587	93.2	6.02	0.0102
185	252.1	26.90	17.9	27.3	0.385	0.0178	0.0457	84.4	15.0	0.00809
190	228.0	24.00	16.1	25.4	0.315	0.0146	0.0376	78.6	20.9	0.00674
195	207.2	21.40	14.4	23.7	0.270	0.0125	0.0324	75.7	23.9	0.00589
200	189.1	19.10	13.0	22.0	0.238	0.0110	0.0287	74.1	25.6	0.00526

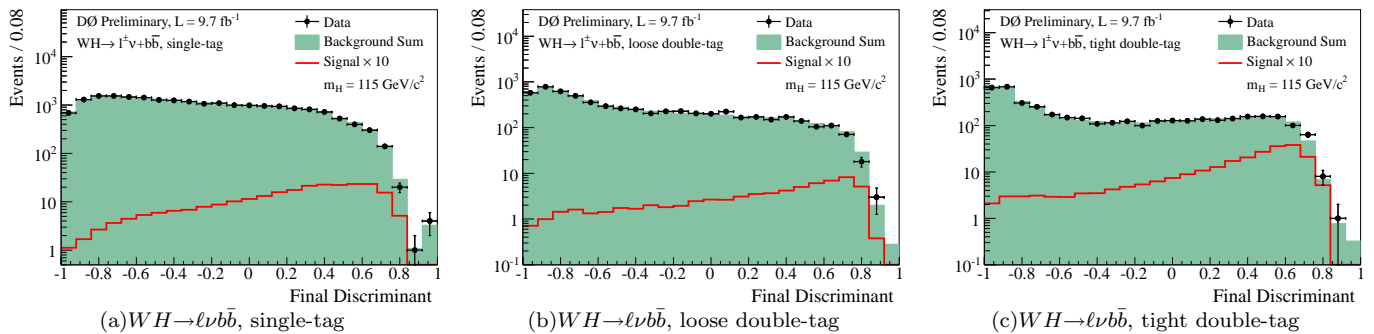


FIG. 1: Final discriminant distribution for the $WH \rightarrow \ell\nu b\bar{b}$ analysis for (a) single-tag, (b) loose double-tag, and (c) tight double-tag samples (summed over any other sub-channels).

A. Final Variable Preparation

The final variables for all analyses (See Table I) are shown in Figs. 1-8. In several of these figures, multiple contributing sub-processes of common sources are summed together. All analyses are performed on a Higgs boson mass grid with steps of 5 GeV/ c^2 .

B. Systematic Uncertainties

The systematic uncertainties differ between analyses for both the signals and backgrounds [6–15]. Here we summarize only the largest contributions. Most analyses carry an uncertainty on the integrated luminosity of 6.1% [54], while the overall normalization of other analyses is determined from the NNLO Z/γ^* cross section in data events near the peak of $Z \rightarrow \ell\ell$ decays. The $H \rightarrow b\bar{b}$ analyses have an uncertainty on the b -tagging rate of 1-10%. These analyses also have an uncertainty on the jet measurement and acceptances of $\sim 7\%$. All analyses include uncertainties associated with lepton measurement and acceptances, which range from 1-9% depending on the final state. The largest contribution for all analyses is the uncertainty on the background cross sections at 4-30% depending on

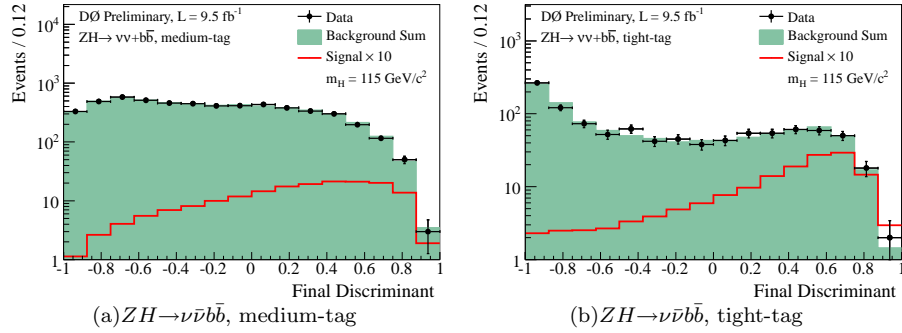


FIG. 2: Final variable distribution for the $ZH \rightarrow \nu\bar{\nu}b\bar{b}$ analyses in (a) medium-tag and (b) tight-tag samples (summed over any other sub-channels).

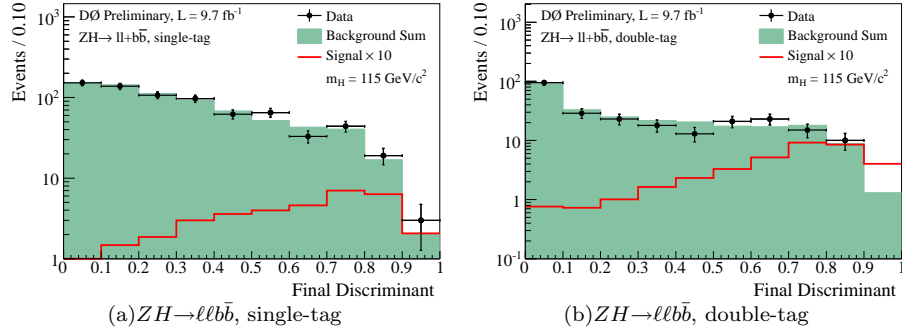


FIG. 3: Final variable distribution for the $ZH \rightarrow \ell\ell b\bar{b}$ analyses in (a) single-tag and (b) double-tag samples (summed over any other sub-channels).

the analysis channel and specific background. These values include both the uncertainty on the theoretical cross section calculations and the uncertainties on the higher-order correction factors. The uncertainty on the expected multijet background is dominated by the statistics of the data sample from which it is estimated, and is considered separately from the other cross section uncertainties as discussed in Sec III B. All analyses take into the uncertainties on the theoretical production cross sections for the different signal processes due to PDF model and scale choice. The $H \rightarrow W^+W^- \rightarrow \ell^+\nu\ell^-\nu$ ($\ell = e, \mu$) analyses divide the data by jet multiplicity and, as discussed, apply different uncertainties on the gluon-gluon fusion Higgs production cross section for each jet multiplicity final state. In addition, several analyses incorporate uncertainties that alter the differential distributions and kinematics of the dominant backgrounds in the analyses. These shapes are derived from the potential variations of the final variables due to generator and background modeling uncertainties. Further details on the systematic uncertainties are given in

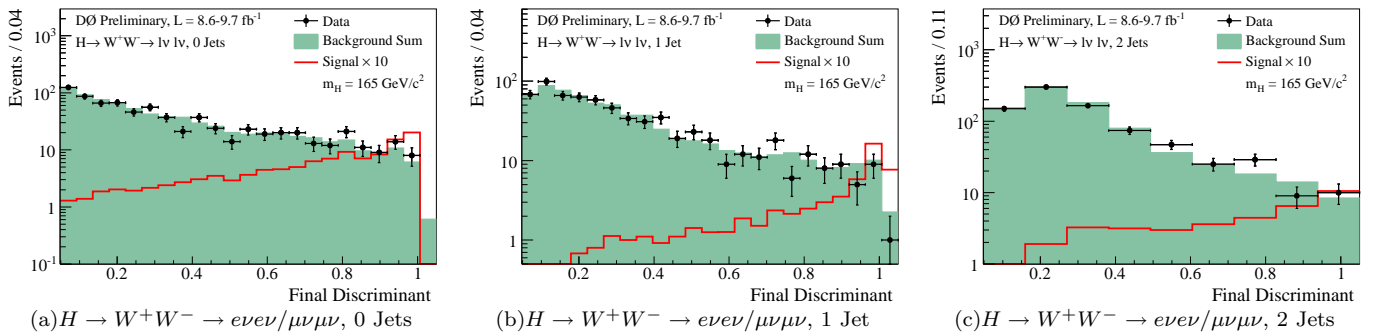


FIG. 4: Final variable distribution for the $H \rightarrow W^+W^- \rightarrow e\nu/\mu\nu\mu\nu$ analyses with (1) 0, (b) 1, and (c) 2 jets in the final state (summed over any other sub-channels).

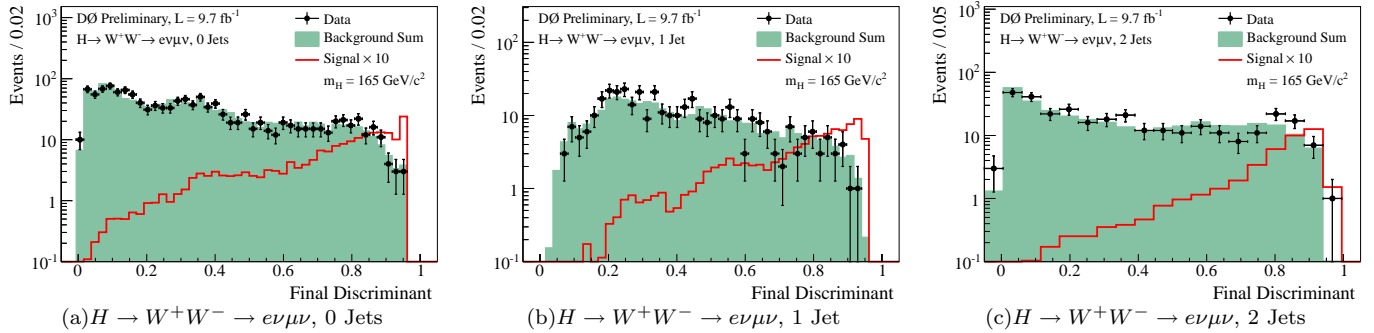


FIG. 5: Final variable distribution for the $H \rightarrow W^+W^- \rightarrow e\nu\mu\nu$ analyses with (a) 0, (b) 1, and (c) 2 jets in the final state (summed over any other sub-channels).

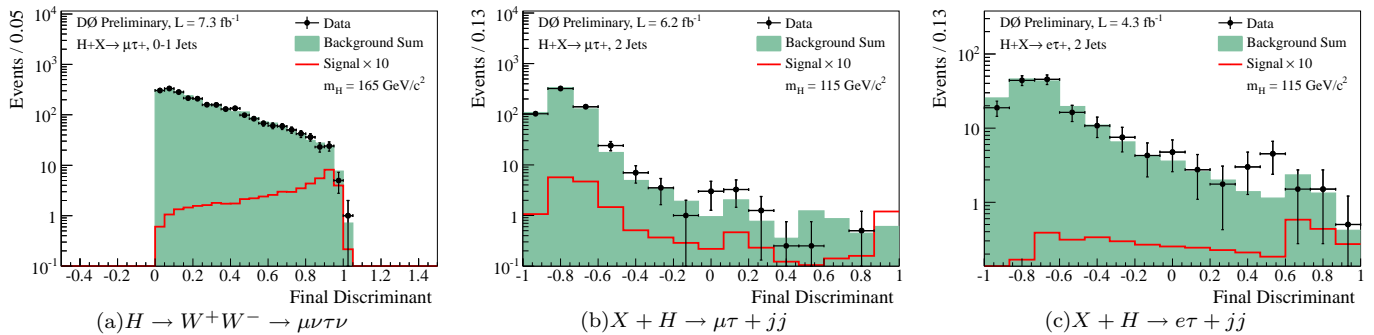


FIG. 6: Final variable distribution for (a) the $H \rightarrow W^+W^- \rightarrow \mu\nu\tau\nu$ analysis, (b) the $X + H \rightarrow \mu\tau + jj$ analysis, and (c) the $X + H \rightarrow e\tau + jj$ analysis (summed over any other sub-channels).

Appendix A.

The systematic uncertainties for background rates are generally several times larger than the signal expectation itself and are an important factor in the calculation of limits. Each systematic uncertainty is folded into the signal and background expectations in the limit calculation via Gaussian distributions. These Gaussian values are sampled for each Monte Carlo (MC) trial (pseudo-experiment) using Poisson distributions for the number of signal and background events. Several of the systematic uncertainties, for example the jet energy scale uncertainty, typically impact the shape of the final variable. These variations in the final variable distributions were preserved in the description of systematic fluctuations for each Poisson trial. Correlations between systematic sources are carried through in the calculation. For example, the uncertainty on the integrated luminosity is held to be correlated between all signals and backgrounds

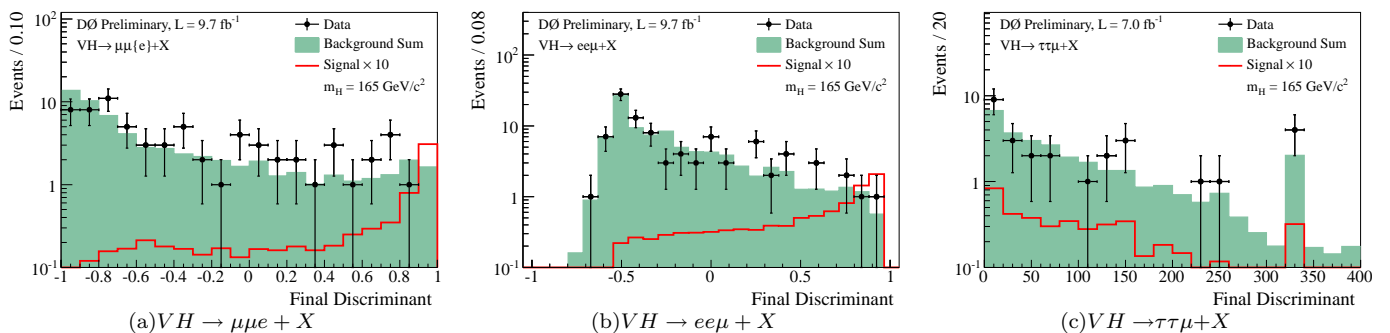


FIG. 7: Final variable distribution for the (a) $VH \rightarrow ee\mu + X$ analysis, (b) $VH \rightarrow \mu\mu e + X$ analysis, and (c) $VH \rightarrow \tau\tau\mu + X$ analysis (summed over any other sub-channels).

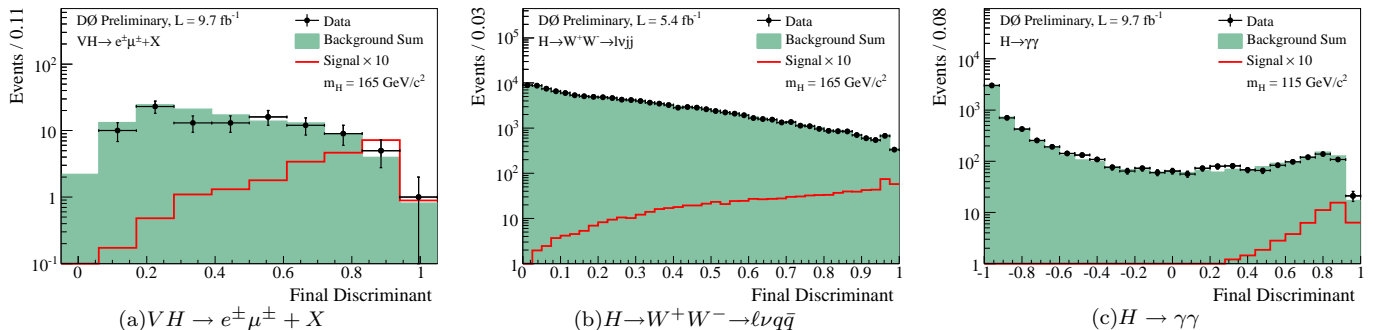


FIG. 8: Final variable distribution for the (a) $VH \rightarrow e^\pm \mu^\pm + X$ analysis, (b) $H \rightarrow W^+ W^- \rightarrow \ell \nu q \bar{q}$ analysis, and (c) $H \rightarrow \gamma \gamma$ analysis (summed over any other sub-channels).

and, thus, the same fluctuation in the luminosity is common to all channels for a single pseudo-experiment. All systematic uncertainties originating from a common source are held to be correlated, as detailed in Table III.

To minimize the degrading effects of systematics on the search sensitivity, the individual background contributions are fitted to the data observation by maximizing a likelihood function for each hypothesis [55]. The likelihood is a joint Poisson probability over the number of bins in the calculation and is a function of the nuisance parameters in the system and their associated uncertainties, which are given an additional Gaussian constraint associated with their prior predictions. The maximization of the likelihood function is performed over the nuisance parameters. A fit is performed to both the background-only (b) and signal-plus-background (s+b) hypothesis separately for each Poisson MC trial.

IV. RESULTS

We derive limits, at 95% C.L., on SM Higgs boson production $\sigma \times BR(H \rightarrow b\bar{b}/W^+W^-/\tau^+\tau^-/\gamma\gamma)$ via individual channels [6–15]. To facilitate model transparency and to accommodate analyses with different degrees of sensitivity, we present our results in terms of the ratio of 95% C.L. upper cross section limits to the SM predicted cross section as a function of Higgs boson mass. The SM prediction for Higgs boson production would therefore be considered excluded at 95% C.L. when this limit ratio falls below unity.

The individual analyses described in Table I are grouped to evaluate combined limits over the range $100 \leq m_H \leq 200 \text{ GeV}/c^2$. The $H+X \rightarrow \ell^\pm \tau_{had}^\mp jj$ analysis contributes to the region $m_H \geq 105 \text{ GeV}/c^2$, the $ZH \rightarrow \ell\ell b\bar{b}$, $ZH \rightarrow \nu\bar{\nu} b\bar{b}$, $WH \rightarrow \ell\nu b\bar{b}$ and $H \rightarrow \gamma\gamma$ analyses contribute for $m_H \leq 150 \text{ GeV}/c^2$, the $VH \rightarrow e^\pm \mu^\pm + X$ and $VH \rightarrow ee\mu/\mu\mu e + X$ analyses contribute for $m_H \geq 115 \text{ GeV}/c^2$, the $VH \rightarrow \tau\tau\mu + X$ analysis contributes for $m_H \geq 100 \text{ GeV}/c^2$, the $H \rightarrow W^+W^- \rightarrow (ee, \mu\mu, e\mu)\nu\nu$ analyses contribute for $m_H \geq 115 \text{ GeV}/c^2$, and the $H \rightarrow W^+W^- \rightarrow \ell\nu q\bar{q}$ analyses contribute for $m_H \geq 155 \text{ GeV}/c^2$.

Figure 9 shows the expected and observed 95% C.L. cross section limits as a ratio to the SM cross section and for the probed mass region ($100 \leq m_H \leq 200 \text{ GeV}/c^2$), with all analyses combined. These results are also summarized in Table IV. The LLR distributions for the full combination are shown in Fig. 10. Included in these figures are the median LLR values for the signal-plus-background hypothesis (LLR_{s+b}), background-only hypothesis (LLR_b), and the observed data (LLR_{obs}). The shaded bands represent the 1 and 2 standard deviation (σ) departures for LLR_b . These distributions can be interpreted as follows:

- The separation between LLR_b and LLR_{s+b} provides a measure of the discriminating power of the search. This is the ability of the analysis to separate the $s+b$ and b -only hypotheses.
- The width of the LLR_b distribution (shown here as one and two standard deviation (σ) bands) provides an estimate of how sensitive the analysis is to a signal-like background fluctuation in the data, taking account of the presence of systematic uncertainties. For example, the analysis sensitivity is limited when a 1σ background fluctuation is large compared to the signal expectation.
- The value of LLR_{obs} relative to LLR_{s+b} and LLR_b indicates whether the data distribution appears to be more like signal-plus-background or background-only. As noted above, the significance of any departures of LLR_{obs}

TABLE III: The correlation matrix for the analysis channels. All uncertainties within a group are considered 100% correlated across channels. The correlated systematic uncertainty on the background cross section (σ) is itself subdivided according to the different background processes in each analysis.

Source	$WH \rightarrow \ell \nu b \bar{b}$	$ZH \rightarrow \nu \bar{\nu} b \bar{b}$	$ZH \rightarrow \ell \ell b \bar{b}$	$H \rightarrow W^+ W^- \rightarrow \ell^\pm \nu \ell^\mp \nu$
Luminosity	×	×		
Normalization				
Jet Energy Scale	×	×	×	×
Jet ID	×	×	×	×
Tau Energy Scale/ID				
Electron ID/Trigger	×	×	×	×
Muon ID/Trigger	×	×	×	×
Photon ID/Trigger				
b -Jet Tagging	×	×	×	
Background σ	×	×	×	×
Background Modeling				
Multijet				
Signal σ	×	×	×	×
Signal modeling				×

Source	$H+X \rightarrow \mu^\pm \tau_{had}^\mp + \leq 1j$	$H+X \rightarrow \ell^\pm \tau_{had}^\mp jj$	$H \rightarrow W^+ W^- \rightarrow \ell \nu q \bar{q}$	$VH \rightarrow VWW$	$H \rightarrow \gamma \gamma$
Luminosity	×	×	×		×
Normalization					
Jet Energy Scale	×	×	×	×	
Jet ID	×	×	×	×	
Tau Energy Scale/ID	×	×			
Electron ID/Trigger	×	×	×	×	
Muon ID/Trigger	×	×	×	×	
Photon ID/Trigger					×
b -Jet Tagging					
Background σ	×	×	×	×	
Background Modeling					
Multijet					
Signal σ	×	×	×	×	×
Signal modeling	×	×	×	×	×

from LLR_b can be evaluated by the width of the LLR_b distribution.

Figure 11 illustrates the exclusion criterion $1 - CL_s$ for the region $100 \leq m_H \leq 200 \text{ GeV}/c^2$. In addition, we provide in Fig. 12 the values for the observed CL_{s+b} and its expected distribution as a function of m_H . The quantity CL_{s+b} is the p -value for the signal-plus-background hypothesis. Figure 13 contains the values for the observed $1-CL_b$, which is the p -value for the background-only hypothesis. These probabilities do not include the look-elsewhere effect (LEE), and are thus local p -values, corresponding to searches for each value of m_H separately. These two p -values (CL_{s+b} and $1-CL_b$) each provide information on the compatibility of their respective hypothesis with the observed data. Small values indicate rejection of the hypothesis and values near unity indicate general agreement between the hypothesis in question and the data. As can be seen in Figure 12, the observed value of CL_{s+b} drops to 2.2% for Higgs masses near $160 \text{ GeV}/c^2$, indicating very small compatibility with the signal-plus-background hypothesis in this mass range. In contrast, the observed value of CL_{s+b} is close to unity at $m_H = 135 \text{ GeV}/c^2$, favoring the signal-plus-background hypothesis. At $m_H = 135 \text{ GeV}/c^2$, the local p -value of $1-CL_b$ is 0.0164, or 2.14 Gaussian standard deviations above the background-only prediction.

We estimate the LEE effect in a simplified manner. In the mass range $100\text{--}125 \text{ GeV}/c^2$, where the low-mass $H \rightarrow b \bar{b}$ searches dominate, the reconstructed mass resolution is approximately 10-15%, or about $15 \text{ GeV}/c^2$. We therefore estimate a trials factor of ~ 2 for the low-mass region. For the high-mass searches, the $H \rightarrow W^+ W^-$ searches dominate the sensitivity. There is little-to-no resolution in reconstructing m_H in these channels due to the presence of two neutrinos in the final state of the most sensitive analyses. We expect a trials factor of approximately two for the high-mass searches. In total, we expect that there are roughly four possible independent locations for uncorrelated excesses to appear in our analysis. The global p -value is therefore $1 - (1 - p_{\min})^4$, using the Dunn-Šidák correction [56]. The global significance for such an excess anywhere in the full mass range is estimated to be $\approx 1.52\sigma$.

As a further investigation of this deviation from the background-only hypothesis, we present in Figure 14 the distribution of the best-fit Higgs boson signal cross section ratio to the SM prediction ($\sigma^{\text{Fit}}/\sigma^{\text{SM}}$). This value is obtained by performing a maximum likelihood fit over all search channels simultaneously, in which the fit is allowed to vary all nuisance parameters within their priors and with the Higgs boson signal rate as a free parameter. The result of this fit, shown along with the ± 1 standard deviation distribution from the fit, yields a best-fit signal rate of roughly twice the SM Higgs boson predicted cross section for $m_H = 135 \text{ GeV}/c^2$, which is consistent with zero rate at two standard deviations. And as expected from Figs 9-13, there is also an excursion from zero cross section near $m_H = 200 \text{ GeV}/c^2$. The p -value for $m_H = 200 \text{ GeV}/c^2$ is 0.0462 (0.95 Gaussian standard deviations above the background-only prediction with the LEE factor).

These two excesses can be studied by separating the contributing sources by Higgs decay: $H \rightarrow b\bar{b}$ and $H \rightarrow W^+W^-$. Figures 15 and 16 show the LLR value for $H \rightarrow b\bar{b}$ and $H \rightarrow W^+W^-$ final states, respectively. Figure 15 includes contributions from $ZH \rightarrow \ell b\bar{b}$, $ZH \rightarrow \nu\nu b\bar{b}$ and $WH \rightarrow \ell\nu b\bar{b}$ searches, and illustrates a small data excess (< 1 standard deviation above expected background) that is nonetheless compatible with the SM Higgs rate for $120 \leq m_H \leq 135 \text{ GeV}/c^2$. Figure 16 includes contributions from $H \rightarrow W^+W^- \rightarrow \ell\nu\ell\nu$, $H \rightarrow W^+W^- \rightarrow \ell\nu jj$ and $VH \rightarrow W^+W^-/ZZ$ searches, and shows a general excess of data somewhat larger than the SM prediction for $m_H \leq 140 \text{ GeV}/c^2$ (≤ 2 standard deviations above the expected background). Figures 17 and 18 show the expected and observed 95% C.L. cross section limits as a ratio to the SM cross section for the probed mass region ($100 \leq m_H \leq 200 \text{ GeV}/c^2$), for $H \rightarrow b\bar{b}$ and $H \rightarrow W^+W^-$ final states, respectively.

TABLE IV: Combined 95% C.L. limits on $\sigma \times BR(H \rightarrow X)$ for SM Higgs boson production. The limits are reported in units of the SM production cross section times branching fraction.

m_H	100	105	110	115	120	125	130	135	140	145	150	155	160	165	170	175	180	185	190	195	200
Expected:	1.25	1.34	1.47	1.58	1.75	1.85	1.82	1.76	1.66	1.49	1.30	1.13	0.81	0.76	0.94	1.12	1.33	1.63	2.09	2.42	2.75
Observed:	1.10	1.20	1.96	2.17	2.69	2.53	3.35	3.49	2.76	2.02	1.84	1.67	0.91	0.94	1.24	1.52	1.81	2.23	3.01	3.83	4.84

V. CONCLUSIONS

We have presented upper limits on standard model Higgs boson production derived from a range of Higgs search analyses including data corresponding to 4.3 - 9.7 fb^{-1} (See Table I). We have combined these analyses leading to new limits more sensitive than each individual limit. The observed 95% C.L. upper limits are found to be a factor of 2.17 (0.94) times the predicted standard model cross section at $m_H = 115(165) \text{ GeV}/c^2$, while the expected limit is found to be a factor of 1.58 (0.76) times the standard model prediction for the same mass(es). We exclude at the 95% C.L. the region $159 < m_H < 166 \text{ GeV}/c^2$ with an *a priori* expected exclusion of $157 < m_H < 172 \text{ GeV}/c^2$. In the mass range $\sim 115 - 145 \text{ GeV}/c^2$, the data exhibit an excess above the background prediction at the level of 1-2 Gaussian standard deviations. The results presented here supersede the previous $D\bar{O}$ combination results [18], with which they are found to be consistent given the increased datasets and improvements to intrinsic sensitivity in the various contributing analyses.

Acknowledgments

We thank the staffs at Fermilab and collaborating institutions, and acknowledge support from the DOE and NSF (USA); CEA and CNRS/IN2P3 (France); MON, Rosatom and RFBR (Russia); CNPq, FAPERJ, FAPESP and FUNDUNESP (Brazil); DAE and DST (India); Colciencias (Colombia); CONACyT (Mexico); NRF (Korea); FOM (The Netherlands); STFC and the Royal Society (United Kingdom); MSMT and GACR (Czech Republic); BMBF and DFG (Germany); SFI (Ireland); The Swedish Research Council (Sweden); and CAS and CNSF (China).

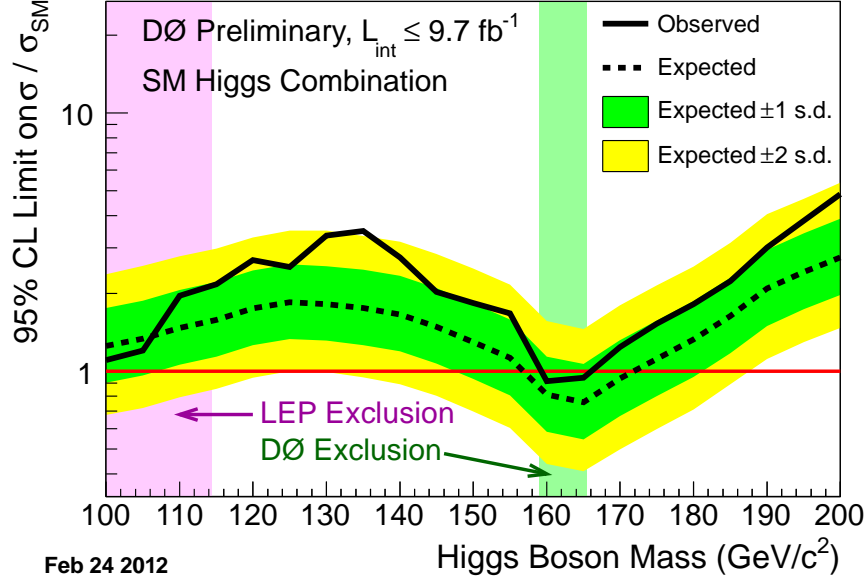


FIG. 9: Expected (median) and observed 95% C.L. cross section upper limit ratios for the combined $WH/ZH/H, H \rightarrow b\bar{b}/W^+W^-/\gamma\gamma/\tau^+\tau^-$ analyses over the $100 \leq m_H \leq 200$ GeV/c^2 mass range. The green and yellow bands correspond to the regions enclosing 1 and 2 standard deviation fluctuations of the background, respectively.

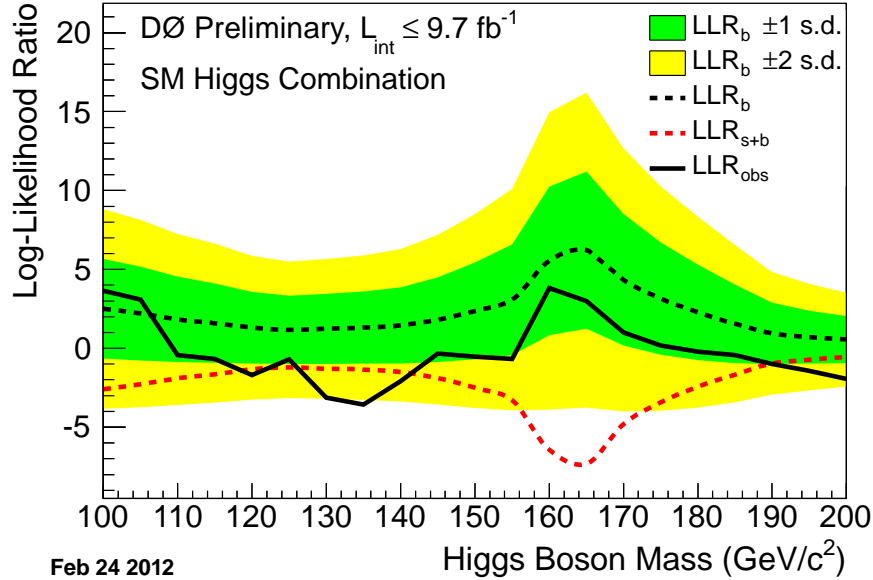


FIG. 10: Log-likelihood ratio distribution for the combined $WH/ZH/H, H \rightarrow b\bar{b}/W^+W^-/\gamma\gamma/\tau^+\tau^-$ analyses over the $100 \leq m_H \leq 200$ GeV/c^2 mass range. The green and yellow bands correspond to the regions enclosing 1 and 2 standard deviation fluctuations of the background, respectively.

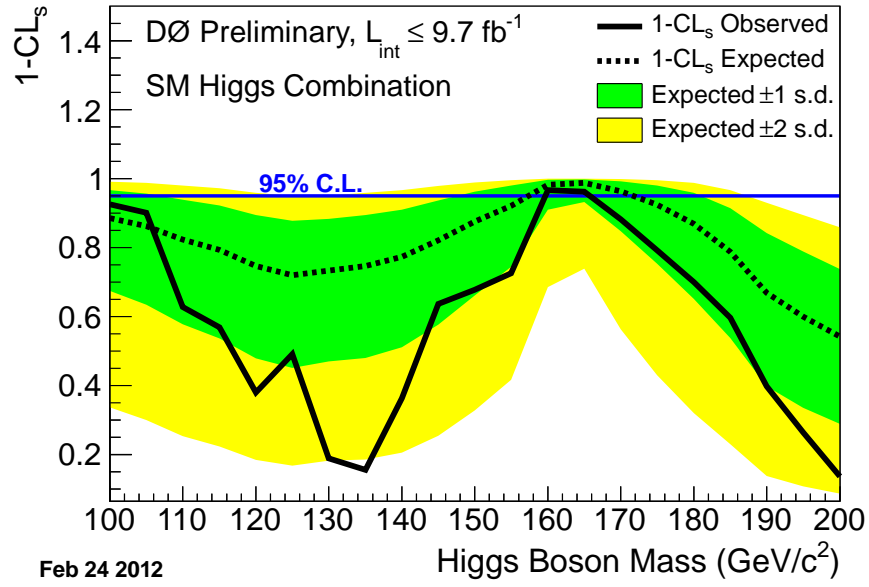


FIG. 11: The $1 - CL_S$ (exclusion probability) distribution for the combined $WH/ZH/H, H \rightarrow b\bar{b}/W^+W^-/\gamma\gamma/\tau^+\tau^-$ analyses over the $100 \leq m_H \leq 200 \text{ GeV}/c^2$ mass range. The green and yellow bands correspond to the regions enclosing 1 and 2 standard deviation fluctuations of the background, respectively.

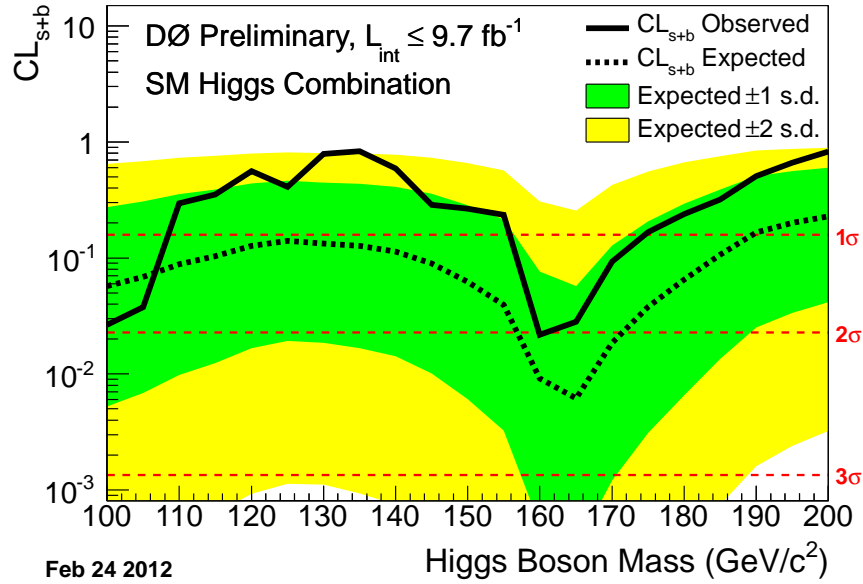


FIG. 12: The CL_{s+b} (signal-plus-background p -value) distribution for the combined $WH/ZH/H, H \rightarrow b\bar{b}/W^+W^-/\gamma\gamma/\tau^+\tau^-$ analyses over the $100 \leq m_H \leq 200 \text{ GeV}/c^2$ mass range. The green and yellow bands correspond to the regions enclosing 1 and 2 standard deviation fluctuations of the background, respectively. The three horizontal dashed lines indicate the p -values corresponding to significances of 1, 2 and 3 standard deviations.

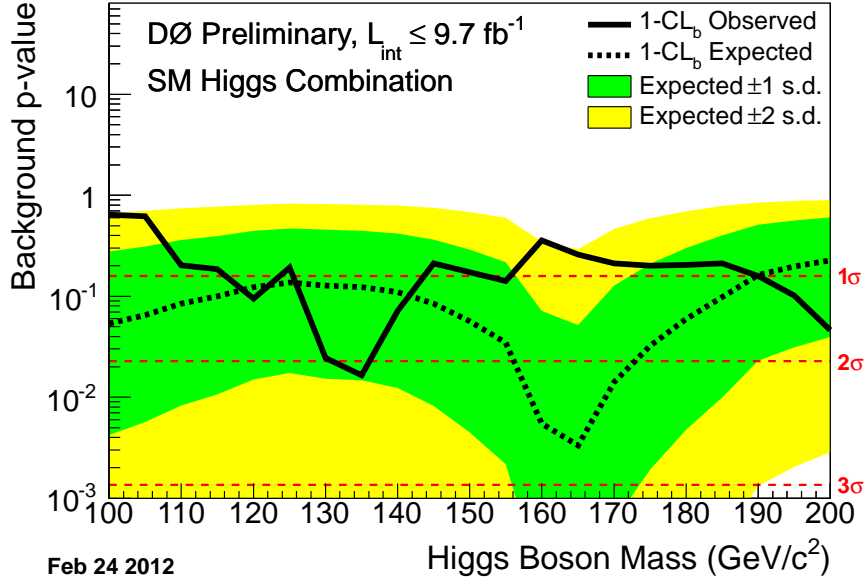


FIG. 13: The $1 - CL_b$ (background p -value) distribution for the combined $WH/ZH/H, H \rightarrow b\bar{b}/W^+W^-/\gamma\gamma/\tau^+\tau^-$ analyses over the $100 \leq m_H \leq 200 \text{ GeV}/c^2$ mass range. Also shown is the expected background p -value for the SM Higgs signal (dotted line). The three horizontal dashed lines indicate the p -values corresponding to significances of 1, 2 and 3 standard deviations.

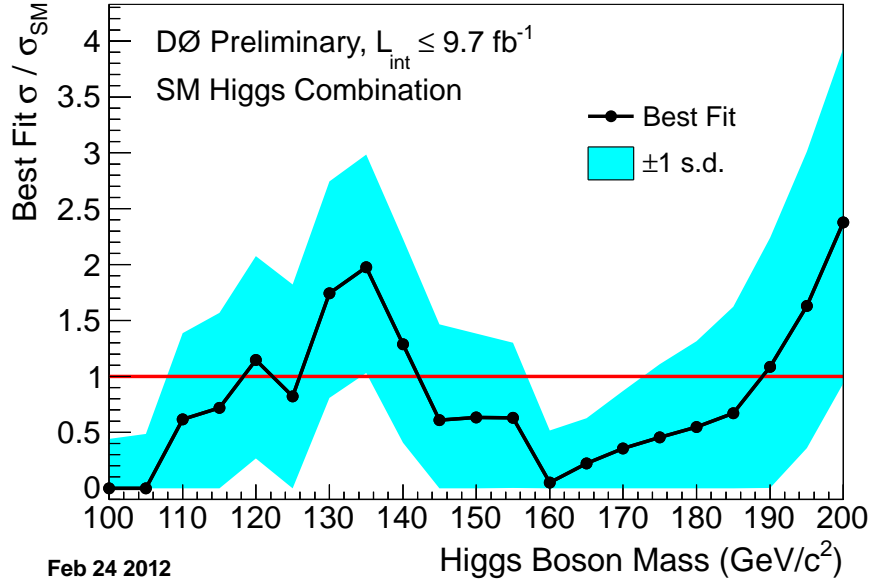


FIG. 14: The best-fit signal cross section ratio to the standard model Higgs prediction (σ^{Fit}/σ^{SM}) for the combined $WH/ZH/H, H \rightarrow b\bar{b}/W^+W^-/\gamma\gamma/\tau^+\tau^-$ analyses over the $100 \leq m_H \leq 200 \text{ GeV}/c^2$ mass range.. This value indicates the value of the Higgs cross section that would best match the observed data in a global fit over all nuisance parameters. The Higgs cross section is treated as a free parameter, bounded at zero. The light-blue band indicates the ± 1 standard deviation region from the fit.

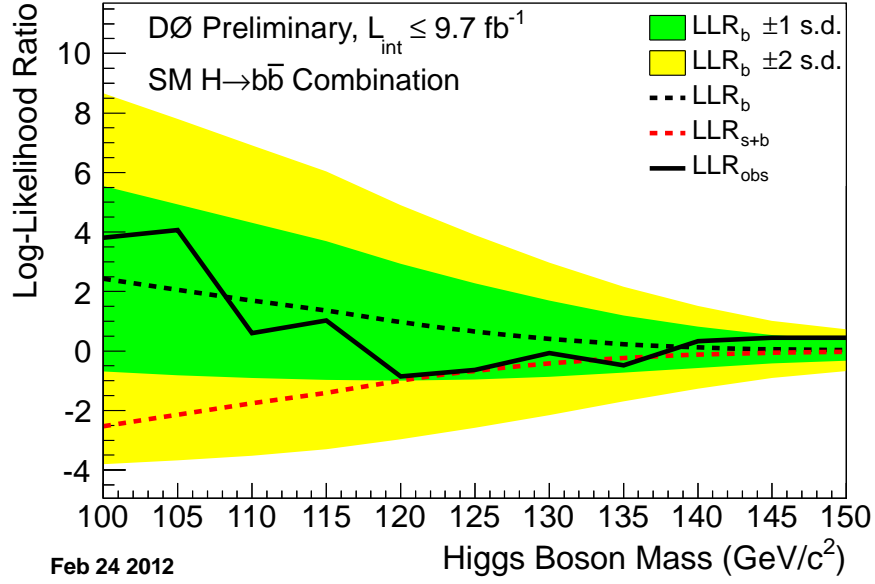


FIG. 15: Log-likelihood ratio distribution for the combined $WH/ZH, H \rightarrow b\bar{b}$ analyses over the $100 \leq m_H \leq 150 \text{ GeV}/c^2$ mass range. The green and yellow bands correspond to the regions enclosing 1 and 2 standard deviation fluctuations of the background, respectively.

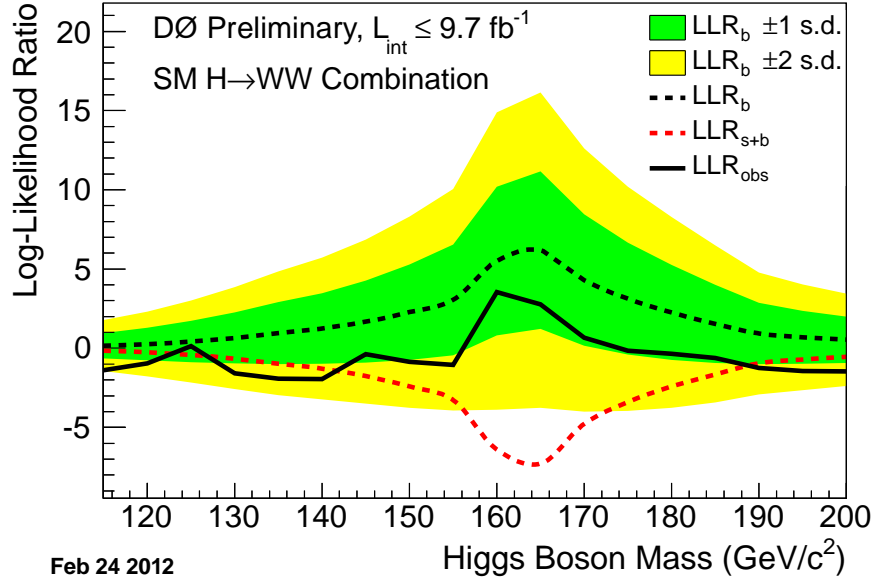


FIG. 16: Log-likelihood ratio distribution for the combined $WH/ZH/H, H \rightarrow W^+W^-$ analyses over the $115 \leq m_H \leq 200 \text{ GeV}/c^2$ mass range. The green and yellow bands correspond to the regions enclosing 1 and 2 standard deviation fluctuations of the background, respectively.

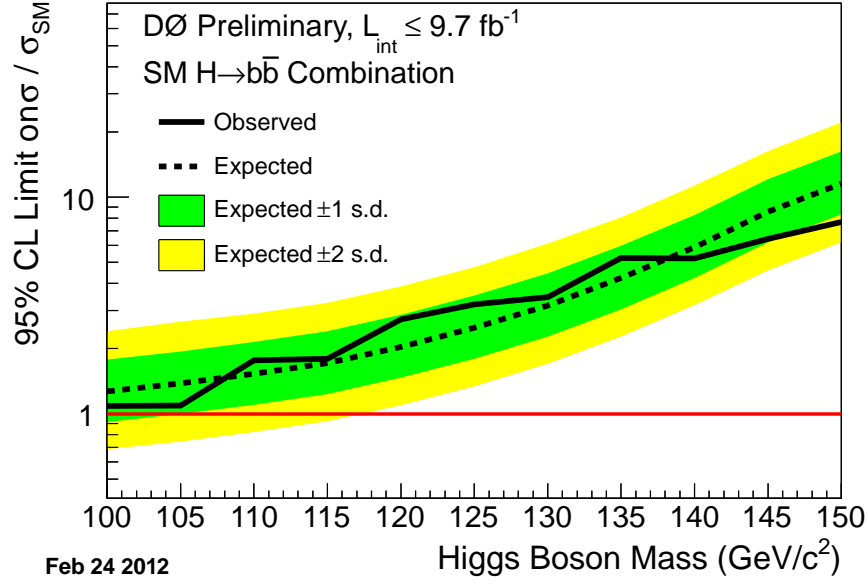


FIG. 17: Expected (median) and observed 95% C.L. cross section upper limit ratios for the combined $WH/ZH, H \rightarrow b\bar{b}$ analyses over the $100 \leq m_H \leq 200 \text{ GeV}/c^2$ mass range. The green and yellow bands correspond to the regions enclosing 1 and 2 standard deviation fluctuations of the background, respectively.

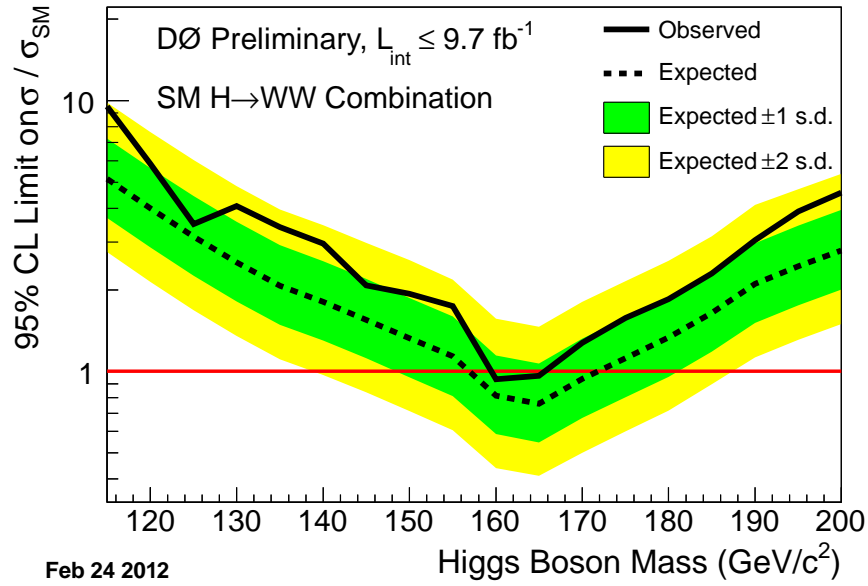


FIG. 18: Expected (median) and observed 95% C.L. cross section upper limit ratios for the combined $WH/ZH/H, H \rightarrow W^+W^-$ analyses over the $100 \leq m_H \leq 200 \text{ GeV}/c^2$ mass range. The green and yellow bands correspond to the regions enclosing 1 and 2 standard deviation fluctuations of the background, respectively.

-
- [1] R. Barate *et al.* [LEP Working Group for Higgs boson searches], Phys. Lett. B **565**, 61 (2003), [arXiv:hep-ex/0306033].
- [2] The LEP Electroweak Working Group, "Status of July 2011", <http://lepewwg.web.cern.ch/LEPEWWG/>.
- [3] CMS Collaboration, arXiv:1202.1488 [hep-ex] (2012); CMS Collaboration, arXiv:1202.4195 [hep-ex] (2012).
- [4] ATLAS Collaboration, Phys. Rev. Lett. **107** (2011) 231801 [arXiv:1109.3615 [hep-ex]]; ATLAS Collaboration, arXiv:1202.1408 (2012).
- [5] V. M. Abazov *et al.* (D0 Collaboration), Nucl. Instrum. Methods Phys. Res. A **565**, 463 (2006); M. Abolins *et al.*, Nucl. Instrum. Methods Phys. Res. A **584**, 75 (2008); R. Angstadt *et al.*, Nucl. Instrum. Methods Phys. Res. A **622**, 298 (2010).
- [6] DØ Collaboration, DØ Note 6309-CONF (2012).
- [7] DØ Collaboration, DØ Note 6299-CONF (2012).
- [8] DØ Collaboration, DØ Note 6296-CONF (2012).
- [9] DØ Collaboration, DØ Note 6302-CONF (2012).
- [10] DØ Collaboration, Phys. Rev. Lett. **106** (2011) 171802 [arXiv:1101.6079v2 [hep-ph]].
- [11] DØ Collaboration, DØ Note 6305-CONF (2012).
- [12] DØ Collaboration, DØ Note 6301-CONF (2012).
- [13] DØ Collaboration, DØ Note 6276-CONF (2012).
- [14] DØ Collaboration, DØ Note 6286-CONF (2012).
- [15] DØ Collaboration, DØ Note 6295-CONF (2012).
- [16] All DØ conference notes are available from:
<http://www-d0.fnal.gov/Run2Physics/WWW/results/higgs.htm>.
- [17] V. M. Abazov *et al.* (D0 Collaboration), Nucl. Instrum. Methods Phys. Res. A **620**, 490 (2010) [arXiv:1002.4224].
- [18] DØ Collaboration, DØ Note 6229-CONF (2012).
- [19] T. Sjöstrand, L. Lonnblad and S. Mrenna, arXiv:hep-ph/0108264 (2001).
- [20] M. L. Mangano, M. Moretti, F. Piccinini, R. Pittau and A. D. Polosa, JHEP **0307**, 001 (2003). [arXiv:hep-ph/0206293].
- [21] CompHEP, E. Boos *et al.*, Nucl. Instrum. Methods Phys. Res. A **534**, 250 (2004); E. Boos, V. Bunichev, L. Dudko, V. Savrin, and A. Sherstnev, Phys. Atom. Nucl. **69**, 1317 (2006).
- [22] J. Campbell and R. K. Ellis, <http://mcfm.fnal.gov/>.
J. M. Campbell, R. K. Ellis, Nucl. Phys. Proc. Suppl. **205-206**, 10-15 (2010). [arXiv:1007.3492 [hep-ph]].
- [23] U. Langenfeld, S. Moch and P. Uwer, Phys. Rev. D **80**, 054009 (2009)
- [24] N. Kidonakis, Phys. Rev. D **74**, 114012 (2006).
- [25] The CDF and DØ Collaborations and the TEVNPHWG Working Group, "Combined CDF and D0 Upper Limits on Standard Model Higgs-Boson Production with up to 8.2 fb⁻¹ of Data", FERMILAB-CONF-11-044-E, CDF Note 10441, DØ Note 6184.
The CDF and DØ Collaborations and the TEVNPHWG Working Group, "Combined CDF and D0 Upper Limits on Standard Model Higgs-Boson Production with up to 8.6 fb⁻¹ of Data", FERMILAB-CONF-11-354-E, CDF Note 10606, DØ Note 6226.
- [26] H. L. Lai *et al.*, Phys. Rev D **55**, 1280 (1997); P. M. Nadolsky *et al.*, Phys. Rev. D **78**, 013004 (2008).
- [27] G. Bozzi, S. Catani, D. de Florian, and M. Grazzini, Phys. Lett. B **564**, 65 (2003); G. Bozzi, S. Catani, D. de Florian, and M. Grazzini, Nucl. Phys. B **737**, 73 (2006).
- [28] C. Balazs, J. Huston, I. Puljak, Phys. Rev. D **63** 014021 (2001).
C. Balazs and C.-P. Yuan, Phys. Lett. B **478** 192-198 (2000).
Qing-Hong Cao and Chuan-Ren Chen, Phys. Rev. D **76** 073006 (2007).
- [29] C. Anastasiou, R. Boughezal and F. Petriello, JHEP **0904**, 003 (2009).
- [30] D. de Florian and M. Grazzini, Phys. Lett. B **674**, 291 (2009).
- [31] M. Grazzini, private communication (2010).
- [32] The CDF and DØ Collaborations and the Tevatron Electroweak Working Group, arXiv:1007.3178 [hep-ex], arXiv:0903.2503 [hep-ex].
- [33] R. V. Harlander and W. B. Kilgore, Phys. Rev. Lett. **88**, 201801 (2002).
- [34] C. Anastasiou and K. Melnikov, Nucl. Phys. B **646**, 220 (2002).
- [35] V. Ravindran, J. Smith, and W. L. van Neerven, Nucl. Phys. B **665**, 325 (2003).
- [36] S. Actis, G. Passarino, C. Sturm, and S. Uccirati, Phys. Lett. B **670**, 12 (2008).
- [37] U. Aglietti, R. Bonciani, G. Degrassi, A. Vicini, arXiv:hep-ph/0610033v1 (2006).
- [38] S. Catani, D. de Florian, M. Grazzini and P. Nason, JHEP **0307**, 028 (2003) [arXiv:hep-ph/0306211].
- [39] A. D. Martin, W. J. Stirling, R. S. Thorne and G. Watt, Eur. Phys. J. C **63**, 189 (2009).
- [40] <http://www.hep.ucl.ac.uk/pdf4lhc/>;
S. Alekhin *et al.*, (PDF4LHC Working Group), [arXiv:1101.0536v1 [hep-ph]];
M. Botje *et al.*, (PDF4LHC Working Group), [arXiv:1101.0538v1 [hep-ph]].
- [41] I. W. Stewart, F. J. Tackmann, [arXiv:1107.2117 [hep-ph]].
- [42] R. D. Ball *et al.* [NNPDF Collaboration], Nucl. Phys. B **809**, 1 (2009) [Erratum-ibid. B **816**, 293 (2009)] [arXiv:0808.1231

[hep-ph]].

- [43] C. Anastasiou, G. Dissertori, M. Grazzini, F. Stöckli and B. R. Webber, JHEP **0908**, 099 (2009). [arXiv:0905.3529 [hep-ph]].
- [44] J. M. Campbell, R. K. Ellis, C. Williams, Phys. Rev. **D81**, 074023 (2010). [arXiv:1001.4495 [hep-ph]].
- [45] J. Baglio and A. Djouadi, JHEP **1010**, 064 (2010) [arXiv:1003.4266v2 [hep-ph]].
- [46] The Fortran program can be found on Michael Spira's web page <http://people.web.psi.ch/~mspira/proglist.html>.
- [47] O. Brein, A. Djouadi, and R. Harlander, Phys. Lett. B **579**, 149 (2004).
- [48] M. L. Ciccolini, S. Dittmaier, and M. Kramer, Phys. Rev. D **68**, 073003 (2003).
- [49] P. Bolzoni, F. Maltoni, S.-O. Moch, and M. Zaro, Phys. Rev. Lett. **105**, 011801 (2010) [arXiv:1003.4451v2 [hep-ph]].
- [50] M. Ciccolini, A. Denner, and S. Dittmaier, Phys. Rev. Lett. **99**, 161803 (2007) [arXiv:0707.0381 [hep-ph]];
M. Ciccolini, A. Denner, and S. Dittmaier, Phys. Rev. D **77**, 013002 (2008) [arXiv:0710.4749 [hep-ph]].
We would like to thank the authors of the HAWK program for adapting it to the Tevatron.
- [51] A. Djouadi, J. Kalinowski and M. Spira, Comput. Phys. Commun. **108**, 56 (1998).
- [52] J. Baglio and A. Djouadi, arXiv:1012.0530 [hep-ph] (2010).
- [53] T. Junk, Nucl. Instrum. Methods Phys. Res. A **434**, 435 (1999); A.Read, CERN 2000-005 (30 May 2000).
- [54] T. Andeen *et al.*, Report No. FERMILAB-TM-2365 (2007).
- [55] W. Fisher, FERMILAB-TM-2386-E (2006).
- [56] Dunn, O.J., "Multiple Comparisons Among Means" Journal of the American Statistical Association, **56**, 52-64 (1961).

Appendices

APPENDIX A: SYSTEMATIC UNCERTAINTIES

TABLE V: Systematic uncertainties on the signal and background contributions for D0's $WH \rightarrow \ell\nu b\bar{b}$ single and double tag channels. Systematic uncertainties are listed by name, see the original references for a detailed explanation of their meaning and on how they are derived. Systematic uncertainties for WH shown in this table are obtained for $m_H = 115 \text{ GeV}/c^2$. Uncertainties are relative, in percent, and are symmetric unless otherwise indicated. Shape uncertainties are labeled with an "(S)", and "SH" represents shape only uncertainty.

$WH \rightarrow \ell\nu b\bar{b}$ Single Tag (TST) channels relative uncertainties (%)

Contribution	Dibosons	$W + b\bar{b}/c\bar{c}$	$W+l.f.$	$t\bar{t}$	single top	Multijet	WH
Luminosity	6.1	6.1	6.1	6.1	6.1	–	6.1
Electron ID/Trigger eff. (S)	1–5	2–4	2–4	1–2	1–2	–	2–3
Muon Trigger eff. (S)	1	1	1	1	1	–	1
Muon ID/Reco eff./resol.	4.1	4.1	4.1	4.1	4.1	–	4.1
Jet ID/Reco eff.	2	2	2	2	2	–	2
Jet Resolution (S)	1–2	2–4	2–3	2–5	1–2	–	2
Jet Energy Scale (S)	4–7	1–5	2–5	2–7	1–2	–	2–6
Vertex Conf. Jet (S)	4–6	3–4	2–3	6–10	2–4	–	3–7
b -tag/taggability (S)	1–3	1–4	7–10	1–6	1–2	–	2–9
Heavy-Flavor K-factor	–	20	–	–	–	–	–
Inst.-WH $e\nu b\bar{b}$ (S)	1–2	2–4	1–3	1–2	1–3	15	1–2
Inst.-WH $\mu\nu b\bar{b}$	–	2.4	2.4	–	–	20	–
Cross Section	6	9	6	7	7	–	6.1
Signal Branching Fraction	–	–	–	–	–	–	1-9
ALPGEN MLM pos/neg(S)	–	SH	–	–	–	–	–
ALPGEN Scale (S)	–	SH	SH	–	–	–	–
Underlying Event (S)	–	SH	–	–	–	–	–
PDF, reweighting	2	2	2	2	2	–	2

$WH \rightarrow \ell\nu b\bar{b}$ Loose Double Tag (LDT) channels relative uncertainties (%)

Contribution	Dibosons	$W + b\bar{b}/c\bar{c}$	$W+l.f.$	$t\bar{t}$	single top	Multijet	WH
Luminosity	6.1	6.1	6.1	6.1	6.1	–	6.1
Electron ID/Trigger eff. (S)	2–5	2–3	2–3	1–2	1–2	–	1–2
Muon Trigger eff. (S)	1	1	1	1	1	–	1
Muon ID/Reco eff./resol.	4.1	4.1	4.1	4.1	4.1	–	4.1
Jet ID/Reco eff.	2	2	2	2	2	–	2
Jet Resolution (S)	1–7	2–7	2–3	2–7	2–4	–	1–5
Jet Energy Scale (S)	2–11	2–5	2–7	2–7	2–5	–	2–8
Vertex Conf. Jet (S)	2–11	2–12	2–3	4–15	2–3	–	3–7
b -tag/taggability (S)	2–15	2–6	6–10	2–5	2–3	–	1–5
Heavy-Flavor K-factor	–	20	–	–	–	–	–
Inst.-WH $e\nu b\bar{b}$ (S)	1–2	2–4	1–3	1–2	1–3	15	1–2
Inst.-WH $\mu\nu b\bar{b}$	–	2.4	2.4	–	–	20	–
Cross Section	6	9	6	7	7	–	6.1
Signal Branching Fraction	–	–	–	–	–	–	1-9
ALPGEN MLM pos/neg(S)	–	SH	–	–	–	–	–
ALPGEN Scale (S)	–	SH	SH	–	–	–	–
Underlying Event (S)	–	SH	–	–	–	–	–
PDF, reweighting	2	2	2	2	2	–	2

$WH \rightarrow \ell\nu b\bar{b}$ Tight Double Tag (TDT) channels relative uncertainties (%)

Contribution	Dibosons	$W + b\bar{b}/c\bar{c}$	$W+l.f.$	$t\bar{t}$	single top	Multijet	WH
Luminosity	6.1	6.1	6.1	6.1	6.1	–	6.1
Electron ID/Trigger eff. (S)	2–5	2–3	2–3	1–2	1–2	–	1–2
Muon Trigger eff. (S)	1	1	1	1	1	–	1
Muon ID/Reco eff./resol.	4.1	4.1	4.1	4.1	4.1	–	4.1
Jet ID/Reco eff.	2	2	2	2	2	–	2
Jet Resolution (S)	2–5	2–4	2–6	2–7	1–2	–	4–6
Jet Energy Scale (S)	3–8	2–5	1–8	2–9	2–4	–	2–6
Vertex Conf. Jet (S)	2–3	2–4	2–5	5–7	2–3	–	2–4
b -tag/taggability (S)	3–15	4–15	10–15	5–10	5–9	–	4–12
Heavy-Flavor K-factor	–	20	–	–	–	–	–
Inst.-WH $e\nu b\bar{b}$ (S)	1–2	2–4	1–3	1–2	1–3	15	1–2
Inst.-WH $\mu\nu b\bar{b}$	–	2.4	2.4	–	–	20	–
Cross Section	6	9	6	7	7	–	6.1
Signal Branching Fraction	–	–	–	–	–	–	1–9
ALPGEN MLM pos/neg(S)	–	SH	–	–	–	–	–
ALPGEN Scale (S)	–	SH	SH	–	–	–	–
Underlying Event (S)	–	SH	–	–	–	–	–
PDF, reweighting	2	2	2	2	2	–	2

TABLE VI: Systematic uncertainty ranges on the signal and background contributions and the error on the total background for D0's $ZH \rightarrow \nu\nu b\bar{b}$ medium-tag and tight-tag channels. Systematic uncertainties are listed by name, see the original references for a detailed explanation of their meaning and on how they are derived. Systematic uncertainties for VH ($WH+ZH$) shown in this table are obtained for $m_H = 115 \text{ GeV}/c^2$. Uncertainties are relative, in percent, and are symmetric unless otherwise indicated. Shape uncertainties are labeled with an “(S)”, and “SH” represents shape only uncertainty.

$ZH \rightarrow \nu\nu b\bar{b}$ medium-tag channel relative uncertainties (%)

Contribution	Top	$V + b\bar{b}/c\bar{c}$	$V+l.f.$	Dibosons	Total Bkgd	VH
Jet ID/Reco Eff (S)	2.0	2.0	2.0	2.0	1.9	2.0
Jet Energy Scale (S)	1.3	1.5	2.8	1.5	1.9	0.3
Jet Resolution (S)	0.5	0.4	0.5	0.8	0.5	0.9
Vertex Conf. / Taggability (S)	3.4	2.2	2.0	2.3	2.2	2.1
b Tagging (S)	1.5	2.6	8.0	3.6	3.7	0.6
Lepton Identification	1.5	0.9	0.8	0.9	0.9	0.9
Trigger	2.0	2.0	2.0	2.0	1.9	2.0
Heavy Flavor Fractions	–	20.0	–	–	8.4	–
Cross Sections	10.0	10.2	10.2	7.0	9.8	7.0
Signal Branching Fraction	–	–	–	–	–	1-9
Luminosity	6.1	6.1	6.1	6.1	5.8	6.1
Multijet Normalization	–	–	–	–	1.1	–
ALPGEN MLM (S)	–	–	SH	–	–	–
ALPGEN Scale (S)	–	SH	SH	–	–	–
Underlying Event (S)	–	SH	SH	–	–	–
PDF, reweighting (S)	SH	SH	SH	SH	SH	SH
Total uncertainty	12.8	23.8	15.1	10.8	14.2	10.0

$ZH \rightarrow \nu\nu b\bar{b}$ tight-tag channel relative uncertainties (%)

Contribution	Top	$V + b\bar{b}/c\bar{c}$	$V+l.f.$	Dibosons	Total Bkgd	VH
Jet ID/Reco Eff (S)	2.0	2.0	2.0	2.0	2.0	2.0
Jet Energy Scale (S)	1.0	1.6	3.9	1.6	1.6	0.5
Jet Resolution (S)	0.7	0.6	2.6	1.4	0.8	1.3
Vertex Conf. / Taggability (S)	3.0	1.9	2.4	2.0	2.3	1.9
b Tagging (S)	8.9	7.3	12.5	6.4	7.4	7.8
Lepton Identification	1.9	0.8	0.3	0.7	1.1	0.8
Trigger	2.0	2.0	2.0	2.0	2.0	2.0
Heavy Flavor Fractions	–	20.0	–	–	11.0	–
Cross Sections	10.0	10.2	10.2	7.0	10.0	7.0
Signal Branching Fraction	–	–	–	–	–	1-9
Luminosity	6.1	6.1	6.1	6.1	6.1	6.1
Multijet Normalization	–	–	–	–	0.2	–
ALPGEN MLM (S)	–	–	SH	–	–	–
ALPGEN Scale (S)	–	SH	SH	–	–	–
Underlying Event (S)	–	SH	SH	–	–	–
PDF, reweighting (S)	SH	SH	SH	SH	SH	SH
Total uncertainty	15.5	24.7	18.3	12.0	16.8	12.7

TABLE VII: Systematic uncertainties on the contributions for D0's $ZH \rightarrow \ell^+ \ell^- b \bar{b}$ channels. Systematic uncertainties are listed by name; see the original references for a detailed explanation of their meaning and on how they are derived. Systematic uncertainties for ZH shown in this table are obtained for $m_H = 115 \text{ GeV}/c^2$. Uncertainties are relative, in percent, and are symmetric unless otherwise indicated. Shape uncertainties are labeled with an "(S)".

$ZH \rightarrow \ell b \bar{b}$ Single Tag (ST) channels relative uncertainties (%)							
Contribution	ZH	Multijet	$Z+l.f.$	$Z+b\bar{b}$	$Z+c\bar{c}$	Dibosons	Top
Jet Energy Scale (S)	4.2	–	6.8	4.9	5.2	6.7	3.3
Jet Energy Resolution (S)	1.2	–	5.2	3.3	3.2	2.2	0.4
Jet ID (S)	0.3	–	0.7	0.3	0.5	0.5	0.6
Taggability (S)	1.5	–	1.0	1.0	1.3	1.3	0.8
Z_{p_T} Model (S)	–	–	2.7	1.4	1.5	–	–
HF Tagging Efficiency (S)	0.4	–	–	1.1	4.0	–	1.3
LF Tagging Efficiency (S)	–	–	73	–	–	3.0	–
ee Multijet Shape (S)	–	54	–	–	–	–	–
Multijet Normalization	–	1-70	–	–	–	–	–
Z +jets Jet Angles (S)	–	–	1.7	2.9	3.4	–	–
AlpGen MLM (S)	–	–	0.3	–	–	–	–
AlpGen Scale (S)	–	–	0.4	0.4	0.4	–	–
Underlying Event (S)	–	–	0.2	0.4	0.3	–	–
Trigger (S)	0.4	–	0.03	0.2	0.2	0.2	0.5
Cross Sections	6	–	–	20	20	7	10
Signal Branching Fraction	1-9	–	–	–	–	–	–
Normalization	2.5	–	0.3	0.3	0.3	2.5	2.5
PDFs	0.6	–	1.0	2.4	1.1	0.7	5.9

$ZH \rightarrow \ell b \bar{b}$ Double Tag (DT) channels relative uncertainties (%)							
Contribution	ZH	Multijet	$Z+l.f.$	$Z+b\bar{b}$	$Z+c\bar{c}$	Dibosons	Top
Jet Energy Scale (S)	2.6	–	7.4	6.5	5.1	5.8	1.0
Jet Energy Resolution(S)	1.0	–	4.0	4.4	4.7	0.9	0.9
JET ID (S)	0.8	–	0.8	0.1	0.1	0.8	0.8
Taggability (S)	0.9	–	0.5	1.0	0.8	0.7	0.9
Z_{p_T} Model (S)	–	–	1.3	1.3	2.0	–	–
HF Tagging Efficiency (S)	5.3	–	–	5.7	5.9	–	4.0
LF Tagging Efficiency (S)	–	–	47	–	–	6.2	–
ee Multijet Shape (S)	–	59	–	–	–	–	–
Multijet Normalization	–	1-70	–	–	–	–	–
Z +jets Jet Angles (S)	–	–	1.4	3.7	3.7	–	–
AlpGen MLM (S)	–	–	0.2	–	–	–	–
AlpGen Scale (S)	–	–	0.3	0.4	0.4	–	–
Underlying Event(S)	–	–	0.3	0.4	0.4	–	–
Trigger (S)	0.4	–	0.4	0.3	0.2	0.3	0.5
Cross Sections	6	–	–	20	20	7	10
Signal Branching Fraction	1-9	–	–	–	–	–	–
Normalization	2.5	–	0.3	0.3	0.3	2.5	2.5
PDFs	0.6	–	1.0	2.4	1.1	0.7	5.9

TABLE VIII: Systematic uncertainties on the signal and background contributions for D0's $H \rightarrow W^+W^- \rightarrow \ell^\pm \ell^\mp$ channels. Systematic uncertainties are listed by name; see the original references for a detailed explanation of their meaning and on how they are derived. Shape uncertainties are labeled with the “s” designation. Systematic uncertainties given in this table are obtained for the $m_H = 165 \text{ GeV}/c^2$ Higgs selection. Cross section uncertainties on the $gg \rightarrow H$ signal depend on the jet multiplicity, as described in the main text. Uncertainties are relative, in percent, and are symmetric unless otherwise indicated.

$H \rightarrow W^+W^- \rightarrow \ell^\pm \ell^\mp$ channels relative uncertainties (%)

Contribution	Dibosons	$Z/\gamma^* \rightarrow \ell\ell$	$W+\text{jet}/\gamma$	$t\bar{t}$	Multijet	$gg \rightarrow H$	$qq \rightarrow qqH$	VH
Luminosity/Normalization	4	–	4	4	4	4	4	4
Cross Section (Scale/PDF)	5-7	–	–	7	–	13-33/8-30	5	6
$Z/\gamma^* \rightarrow \ell\ell$ n-jet norm	–	2-15	–	–	–	–	–	–
$Z/\gamma^* \rightarrow \ell\ell$ MET model	–	5-19	–	–	–	–	–	–
$W+\text{jet}/\gamma$ norm	–	–	6-30	–	–	–	–	–
$W+\text{jet}/\gamma$ ISR/FSR model (s)	–	–	2-20	–	–	–	–	–
Vertex Confirmation (s)	1-5	1-5	1-5	5-6	–	1-5	1-5	1-5
Jet identification (s)	1	1	1	1	–	1	1	1
Jet Energy Scale (s)	1-5	1-5	1-5	1-4	–	1-5	1-5	1-4
Jet Energy Resolution(s)	1-4	1-4	1-4	1-4	–	1-3	1-4	1-3
B-tagging (s)	–	–	–	1-5	–	–	–	–

TABLE IX: Systematic uncertainties on the signal and background contributions for D0's $H \rightarrow W^+W^- \rightarrow \mu\nu\tau_{\text{had}}\nu$ channel. Systematic uncertainties are listed by name; see the original references for a detailed explanation of their meaning and on how they are derived. Shape uncertainties are labeled with the shape designation (S). Systematic uncertainties shown in this table are obtained for the $m_H = 165 \text{ GeV}/c^2$ Higgs selection. Uncertainties are relative, in percent, and are symmetric unless otherwise indicated.

D0: $H \rightarrow W^+W^- \rightarrow \mu\nu\tau_{\text{had}}\nu$ channel relative uncertainties (%)

Contribution	Diboson	$Z/\gamma^* \rightarrow \ell\ell$	$W+\text{jets}$	$t\bar{t}$	Multijet	$gg \rightarrow H$	$qq \rightarrow qqH$	VH
Luminosity ($\sigma_{\text{inel}}(pp)$)	4.6	4.6	–	4.6	–	4.6	4.6	4.6
Luminosity Monitor	4.1	4.1	–	4.1	–	4.1	4.1	4.1
Trigger	5.0	5.0	–	5.0	–	5.0	5.0	5.0
Lepton ID	3.7	3.7	–	3.7	–	3.7	3.7	3.7
EM veto	5.0	–	–	5.0	–	5.0	5.0	5.0
Tau Energy Scale (S)	1.0	1.1	–	<1	–	<1	<1	<1
Jet Energy Scale (S)	8.0	<1	–	1.8	–	2.5	2.5	2.5
Jet identification (S)	<1	<1	–	7.5	–	5.0	5.0	5.0
Multijet (S)	–	–	–	–	20-50	–	–	–
Cross Section (scale/PDF)	7.0	4.0	–	10	–	7/8	4.9	6.1
Signal Branching Fraction	–	–	–	–	–	0-7.3	0-7.3	0-7.3
Modeling	1.0	–	10	–	–	3.0	3.0	3.0

TABLE X: Systematic uncertainties on the signal and background contributions for D0's $H \rightarrow WW^* \rightarrow \ell\nu jj$ electron and muon channels. Systematic uncertainties are listed by name; see the original references for a detailed explanation of their meaning and on how they are derived. Signal uncertainties are shown for $m_H = 160 \text{ GeV}/c^2$ for all channels except for WH , shown for $m_H = 115 \text{ GeV}/c^2$. Those affecting the shape of the RF discriminant are indicated with "Y." Uncertainties are listed as relative changes in normalization, in percent, except for those also marked by "S," where the overall normalization is constant, and the value given denotes the maximum percentage change from nominal in any region of the distribution.

D0: $H \rightarrow WW^* \rightarrow \ell\nu jj$ Run II channel relative uncertainties (%)								
Contribution	Shape	W +jets	Z +jets	Top	Diboson	$gg \rightarrow H$	$qq \rightarrow qqH$	WH
Jet energy scale	Y	$(+6.7)_{-5.4}^S$	< 0.1	± 0.7	± 3.3	$(+5.7)_{-4.0}$	± 1.5	$(+2.7)_{-2.3}$
Jet identification	Y	$\pm 6.6^S$	< 0.1	± 0.5	± 3.8	± 1.0	± 1.1	± 1.0
Jet resolution	Y	$(+6.6)_{-4.1}^S$	< 0.1	± 0.5	$(+1.0)_{-0.5}$	$(+3.0)_{-0.5}$	± 0.8	± 1.0
Association of jets with PV	Y	$\pm 3.2^S$	$\pm 1.3^S$	± 1.2	± 3.2	± 2.9	± 2.4	$(+0.9)_{-0.2}$
Luminosity	N	n/a	n/a	± 6.1	± 6.1	± 6.1	± 6.1	± 6.1
Muon trigger	Y	$\pm 0.4^S$	< 0.1	< 0.1	< 0.1	< 0.1	< 0.1	< 0.1
Electron identification	N	± 4.0	± 4.0	± 4.0	± 4.0	± 4.0	± 4.0	± 4.0
Muon identification	N	± 4.0	± 4.0	± 4.0	± 4.0	± 4.0	± 4.0	± 4.0
ALPGEN tuning	Y	$\pm 1.1^S$	$\pm 0.3^S$	n/a	n/a	n/a	n/a	n/a
Cross Section	N	± 6	± 6	± 10	± 7	± 10	± 10	± 6
Heavy-flavor fraction	Y	± 20	± 20	n/a	n/a	n/a	n/a	n/a
Signal Branching Fraction	N	n/a	n/a	n/a	n/a	0-7.3	0-7.3	0-7.3
PDF	Y	$\pm 2.0^S$	$\pm 0.7^S$	< 0.1 ^S	< 0.1 ^S	< 0.1 ^S	< 0.1 ^S	< 0.1 ^S
			Electron channel			Muon channel		
Multijet Background	Y		± 6.5			± 26		

TABLE XI: Systematic uncertainties on the signal and background contributions for D0's $VH \rightarrow VWW \rightarrow ee\mu, \mu\mu e$ channels. Systematic uncertainties are listed by name; see the original references for a detailed explanation of their meaning and on how they are derived. Shape uncertainties are labeled with the "s" designation. Systematic uncertainties given in this table are obtained for the $m_H = 145 \text{ GeV}$ Higgs selection. Uncertainties are relative, in percent, and are symmetric unless otherwise indicated.

$VH \rightarrow VWW \rightarrow$ Trilepton channels relative uncertainties (%)								
Contribution	Dibosons	$Z/\gamma^* \rightarrow \ell\ell$	W +jet/ γ	$t\bar{t}$	$Z\gamma$	VH	$gg \rightarrow H$	$qq \rightarrow qqH$
Luminosity	6.1	6.1	6.1	6.1	–	6.1	6.1	6.1
Cross Section (Scale/PDF)	6	6	6	7	–	6.2	7	4.9
PDF	2.5	2.5	2.5	2.5	–	2.5	2.5	2.5
Electron Identification	2.5	2.5	2.5	2.5	–	2.5	2.5	2.5
Muon Identification	4	4	4	4	–	4	4	4
Trigger	3.5	3.5	3.5	3.5	–	3.5	3.5	3.5
$Z\gamma$	–	–	–	–	8	–	–	–
V + jets lepton fake rate	–	30	30	–	–	–	–	–
Z - p_T reweighting (s)	–	$\pm 1\sigma$	–	–	–	–	–	–
Electron smearing (s)	$\pm 1\sigma$	$\pm 1\sigma$	$\pm 1\sigma$	$\pm 1\sigma$	–	$\pm 1\sigma$	$\pm 1\sigma$	$\pm 1\sigma$
Muon smearing (s)	$\pm 1\sigma$	$\pm 1\sigma$	$\pm 1\sigma$	$\pm 1\sigma$	–	$\pm 1\sigma$	$\pm 1\sigma$	$\pm 1\sigma$

TABLE XII: Systematic uncertainties on the signal and background contributions for D0's $VH \rightarrow e^\pm \nu_e \mu^\pm \nu_\mu$ ($V = W, Z$) channels. Systematic uncertainties are listed by name; see the original references for a detailed explanation of their meaning and on how they are derived. Shape uncertainties are labeled with the “shape” designation. Systematic uncertainties shown in this table are obtained for the $m_H = 165 \text{ GeV}/c^2$ Higgs selection. Uncertainties are relative, in percent, and are symmetric unless otherwise indicated.

$VH \rightarrow e^\pm \nu_e \mu^\pm \nu_\mu$ like charge electron muon pair channel relative uncertainties (%)						
Contribution	VH	$Z + jet/\gamma$	$W + jet/\gamma$	tt	Diboson	Multijet
Cross section	6.2	–	–	6	7	–
Luminosity/Normalization	4	–	4	4	4	–
Multijet	–	–	–	–	–	30
Trigger	2	2	2	2	2	2
Charge flip	–	50	–	50	50	–
W+jets/ γ	–	–	10	–	–	–
$W - p_T$ model	–	–	shape	–	–	–
$Z - p_T$ model	–	shape	–	–	–	–
W+jets/ γ ISR/FSR model	–	–	shape	–	–	–

TABLE XIII: Systematic uncertainties on the signal and background contributions for D0's $\tau\tau jj$ Run IIB channel. Systematic uncertainties for the Higgs signal shown in this table are obtained for $m_H = 135 \text{ GeV}/c^2$. Systematic uncertainties are listed by name; see the original references for a detailed explanation of their meaning and on how they are derived. Uncertainties are relative, in percent, and are symmetric unless otherwise indicated. Shape uncertainties are labeled with an "(S)."

$\mu\tau_{had}jj$ Run IIB channel relative uncertainties (%)								
Contribution	VH	VBF	ggH	W +jets	Z +jets	Top	Dibosons	Multijet
Luminosity	6.1	6.1	6.1	6.1	6.1	6.1	6.1	–
μ ID	2.9	2.9	2.9	2.9	2.9	2.9	2.9	–
<i>Single</i> μ trigger	5.0	5.0	5.0	5.0	5.0	5.0	5.0	–
inclusive trigger relative	7.0	7.0	7.0	7.0	7.0	7.0	7.0	–
τ energy correction	9.8	9.8	9.8	9.8	9.8	9.8	9.8	–
τ track efficiency	1.4	1.4	1.4	1.4	1.4	1.4	1.4	–
τ selection by type	10,4,5	10,4,5	10,4,5	10,4,5	10,4,5	10,4,5	10,4,5	–
Cross section	6.2	4.9	33	6.0	6.0	10.0	7.0	–
GGF Signal PDF	–	–	29	–	–	–	–	–
GGF H_{pT} Reweighting (S)	–	– ~ 5.0	–	–	–	–	–	–
Signal Branching Fraction	0-7.3	0-7.3	0-7.3	–	–	–	–	–
Vertex confirmation for jets(S)	~ 5.0	~ 5.0	~ 5.0	~ 5.0	~ 5.0	~ 5.0	~ 5.0	–
Jet ID(S)	~ 5	~ 5	~ 5	~ 5	~ 5	~ 5	~ 5	–
Jet Energy Resolution (S)	~ 5	~ 5	~ 5	~ 5	~ 5	~ 5	~ 5	–
Jet energy Scale (S)	~ 5	~ 5	~ 5	~ 5	~ 5	~ 5	~ 5	–
Jet pT	5.5	5.5	5.5	5.5	5.5	5.5	5.5	–
PDF reweighting	1.6	1.6	1.6	1.6	2	2	2	–
Multijet Normalization	–	–	–	–	–	–	–	5.3
Multijet Shape	–	–	–	–	–	–	–	~ 15

$e\tau_{had}jj$ Run IIB relative uncertainties (%)								
Contribution	VH	VBF	ggH	W +jets	Z +jets	Top	Dibosons	Multijet
Luminosity	6.1	6.1	6.1	6.1	6.1	6.1	6.1	–
Electron ID	4	4	4	4	4	4	4	–
Electron trigger	2	2	2	2	2	2	2	–
τ energy correction	9.8	9.8	9.8	9.8	9.8	9.8	9.8	–
τ track efficiency	1.4	1.4	1.4	1.4	1.4	1.4	1.4	–
τ selection by type	10,4,5	10,4,5	10,4,5	10,4,5	10,4,5	10,4,5	10,4,5	–
Cross section	6.1	4.9	33	6.0	6.0	10.0	7.0	–
GGF Signal PDF	–	–	29	–	–	–	–	–
GGF H_{pT} Reweighting (S)	–	–	~ 5.0	–	–	–	–	–
Signal Branching Fraction	0-7.3	0-7.3	0-7.3	–	–	–	–	–
Vertex confirmation for jets(S)	~ 5.0	–						
Jet ID(S)	~ 10	~ 5	–					
Jet Energy Resolution (S)	~ 10	–						
Jet energy Scale (S)	~ 10	–						
Jet pT	5.5	5.5	5.5	5.5	5.5	5.5	5.5	–
PDF reweighting	1.6	1.6	1.6	1.6	2	2	2	–
Multijet Normalization	–	–	–	–	–	–	–	4.7
Multijet Shape	–	–	–	–	–	–	–	~ 15

TABLE XIV: Systematic uncertainties on the signal and background contributions for D0's $\tau\tau\mu + X$ channel. Systematic uncertainties are listed by name; see the original references for a detailed explanation of their meaning and on how they are derived. Shape uncertainties are labeled with the “s” designation. Cross section uncertainties on the $gg \rightarrow H$ signal depend on the jet multiplicity, as described in the main text. Uncertainties are relative, in percent, and are symmetric unless otherwise indicated.

Contribution	Dibosons	Z/γ^*	$t\bar{t}$	Instrumental	$gg \rightarrow H$	$qq \rightarrow qqH$	VH
Luminosity/Normalization	6	6	6	24	6	6	6
Trigger	3	3	3	–	3	3	3
Cross Section (Scale/PDF)	7	6	10	–	13-33/7.6-30	4.9	6.2
PDF	2.5	2.5	2.5	–	2.5	2.5	2.5
Tau Id per τ (Type 1/2/3)	7/3.5/5	7/3.5/5	7/3.5/5	–	7/3.5/5	7/3.5/5	7/3.5/5
Tau Energy Scale	1	1	1	–	1	1	1
Tau Track Match per τ	1.4	1.4	1.4	–	1.4	1.4	1.4
Muon Identification	2.9	2.9	2.9	–	2.9	2.9	2.9

TABLE XV: Systematic uncertainties on the signal and background contributions for D0's $H \rightarrow \gamma\gamma$ channel. Systematic uncertainties for the Higgs signal shown in this table are obtained for $m_H = 125 \text{ GeV}/c^2$. Systematic uncertainties are listed by name; see the original references for a detailed explanation of their meaning and on how they are derived. Uncertainties are relative, in percent, and are symmetric unless otherwise indicated.

Contribution	Background	Signal
Luminosity	6	6
Acceptance	–	2
electron ID efficiency	2	–
electron track-match inefficiency	10	–
Photon ID efficiency	3	3
Photon energy scale	2	1
Cross Section	4	10
Background subtraction	15	–
ONN Shape	1-5	–